HAL
open science

Multiscale Hybrid-Mixed Method for the Stokes and Brinkman Equations – The Method

Rodolfo Araya, Christopher Harder, Abner H. Poza, Frédéric Valentin

▶ **To cite this version:**

Rodolfo Araya, Christopher Harder, Abner H. Poza, Frédéric Valentin. Multiscale Hybrid-Mixed Method for the Stokes and Brinkman Equations – The Method. 2016. hal-01347517

HAL Id: hal-01347517

https://hal.science/hal-01347517v1

Preprint submitted on 21 Jul 2016

HAL is a multi-disciplinary open access archive for the deposit and dissemination of scientific research documents, whether they are published or not. The documents may come from teaching and research institutions in France or abroad, or from public or private research centers.

L'archive ouverte pluridisciplinaire **HAL**, est destinée au dépôt et à la diffusion de documents scientifiques de niveau recherche, publiés ou non, émanant des établissements d'enseignement et de recherche français ou étrangers, des laboratoires publics ou privés.

Multiscale Hybrid-Mixed Method for the Stokes and Brinkman Equations – The Method

Rodolfo Araya[a], Christopher Harder[b], Abner H. Poza[1], Frédéric Valentin[d]

[a] *Departamento de Ingeniería Matemática & CI^{2}MA, Universidad de Concepción, Casilla 160-C, Concepción, Chile*
[b] *Metropolitan State University of Denver, Department of Mathematical and Computer Sciences, P.O. Box 173362, Campus Box 38, Denver, CO 80217-3362, USA*
[c] *Facultad de Ingeniería, Universidad Católica de la Santísima Concepción, Casilla 297, Concepción, Chile*
[d] *Department of Computational and Applied Mathematics, LNCC - National Laboratory for Scientific Computing, Av. Getúlio Vargas, 333, 25651-070 Petrópolis - RJ, Brazil*

Abstract

The multiscale hybrid-mixed (MHM) method is extended to the Stokes and Brinkman equations with highly heterogeneous coefficients. The approach is constructive. We first propose an equivalent dual-hybrid formulation of the original problem using a coarse partition of the heterogeneous domain. Faces may be not aligned with jumps in the data. Then, the exact velocity and the pressure are characterized as the solution of a global face problem and the solutions of local independent Stokes (or Brinkman) problems at the continuous level. Owing to this decomposition, the one-level MHM method stems from the standard Galerkin approach for the Lagrange multiplier space. Basis functions are responsible for upscaling the unresolved scales of the medium into the global formulation. They are the exact solution of the local problems with prescribed Neumann boundary conditions on faces driven by the Lagrange multipliers. We make the MHM method effective by adopting the unusual stabilized finite element method to solve the local problems approximately. As such, equal-order interpolation turns out to be an option for the velocity, the pressure and the Lagrange multipliers. The numerical solutions share the important properties of the continuum, such as local equilibrium with respect to external forces and the local mass conservation. Several academic and highly heterogeneous tests infer that the method achieves super-convergence for the velocity as well as optimal convergence for the pressure and also for the stress tensor in their natural norms.

Keywords: Stokes equation, Brinkman model, mixed method, hybrid method, multiscale finite element
2010 MSC: 65N12, 65N30

1. Introduction

Interesting problems are modeled through the Stokes (Brinkman) operator with coefficients that account for highly heterogenous media. Diverse engineering, geophysics, and hydrology problems involve such a system in which the common characteristic is the wide range of length-scales presented. To be more precise, let $\Omega \subset \mathbb{R}^d$, $d \in \{2, 3\}$, be an open, bounded domain with polygonal boundary $\partial\Omega$. The generalized Stokes problem, also called the Brinkman model, is: find the velocity $\boldsymbol{u}$ and the pressure p such that

$$\begin{aligned} -\nu\,\Delta\boldsymbol{u} + \boldsymbol{\gamma}\,\boldsymbol{u} + \nabla p &= \boldsymbol{f} \quad \text{in } \Omega, \\ \nabla\cdot\boldsymbol{u} &= 0 \quad \text{in } \Omega, \\ \boldsymbol{u} &= \boldsymbol{g} \quad \text{on } \partial\Omega, \end{aligned} \tag{1}$$

Email addresses: `rodolfo.araya@udec.cl` (Rodolfo Araya), `harderc@msudenver.edu` (Christopher Harder), `apoza@ucsc.cl` (Abner H. Poza), `valentin@lncc.br` (Frédéric Valentin)

where $\boldsymbol{f} \in L^2(\Omega)^d$ and $\boldsymbol{g} \in H^{1/2}(\partial\Omega)^d$ with $\int_{\partial\Omega} \boldsymbol{g} \cdot \boldsymbol{n}\, ds = 0$, and $\boldsymbol{n}$ represents the outer normal vector to $\partial\Omega$. The diffusion coefficient ν is a positive constant and the reaction coefficient $\boldsymbol{\gamma}$ is a semidefinite positive, symmetric tensor which is uniformly elliptic, i.e., there exist positive constants c_1, c_2 such that

$$0 \leq c_1\, |\boldsymbol{\xi}|^2 \leq \boldsymbol{\xi}^T \boldsymbol{\gamma}(\boldsymbol{x})\, \boldsymbol{\xi} \leq c_2\, |\boldsymbol{\xi}|^2 \quad \text{for all } \boldsymbol{\xi} \in \mathbb{R}^d \text{ and } \boldsymbol{x} \in \Omega, \tag{2}$$

and $\boldsymbol{\gamma}(\boldsymbol{x})$ may contain multiscale geometrical features of the media ($c_1 > 0$ if $\boldsymbol{\gamma}$ is a definite positive matrix). We recognize the Stokes problem in (1) if $\boldsymbol{\gamma} = \boldsymbol{0}$. The Dirichlet boundary condition in (1) is chosen for sake of simplicity, and Neumann or Robin boundary conditions can be easily accommodated in what follows.

The standard variational mixed formulation associated to (1) reads: Find $\boldsymbol{u} \in H^1(\Omega)^d$, with $\boldsymbol{u} = \boldsymbol{g}$ on $\partial\Omega$, and $p \in L^2_0(\Omega)$ such that

$$\begin{aligned} a(\boldsymbol{u}, \boldsymbol{v}) + b(\boldsymbol{v}, p) &= (\boldsymbol{f},\, \boldsymbol{v})_\Omega \quad \text{for all } \boldsymbol{v} \in H^1_0(\Omega)^d, \\ b(\boldsymbol{u}, q) &= 0 \quad \text{for all } q \in L^2_0(\Omega), \end{aligned} \tag{3}$$

where the bilinear forms $a(\cdot,\cdot)$ and $b(\cdot,\cdot)$ are defined by

$$a(\boldsymbol{w}, \boldsymbol{v}) \;:=\; (\nu\, \nabla \boldsymbol{w}, \nabla \boldsymbol{v})_\Omega + (\boldsymbol{\gamma}\, \boldsymbol{w}, \boldsymbol{v})_\Omega \quad \text{and} \quad b(\boldsymbol{v}, q) \;:=\; -(\nabla \cdot \boldsymbol{v}, q)_\Omega, \tag{4}$$

for all $\boldsymbol{w}$, $\boldsymbol{v} \in H^1(\Omega)^d$ and $q \in L^2_0(\Omega)$. Hereafter the spaces have their usual meaning and $(\cdot,\cdot)_D$ stands for the L^2 inner product on a set $D \subset \mathbb{R}^d$.

Numerical methods for (3) have long been an important subject for numericists. Aside from its practical importance, model (3) has attracted great attention due to its mixed character, which demands a deep understanding of the compatibility condition between the velocity and pressure spaces, as well as for its singularly perturbed behavior when the reaction term dominates. Unfortunately, the desirable features of numerical methods (stability, optimality and robustness) are not enough to handle realistic three-dimensional highly heterogeneous problems. Particularly, standard (stable and stabilized) finite element methods are no longer an option since they lack cost-effectiveness when employed for multiscale problems. In fact, an extremely fine mesh is mandatory to account for the multiple scale features of the media, which still makes these computations out of reach of the modern parallel architectures.

The goal is to keep the aforementioned (desirable) properties of the standard (stable or stabilized) finite element methods valid on coarse meshes. It is then necessary to embed upscaling processes in the construction of the numerical methods. In this context, the multiscale finite element method is a competitive option. First proposed and analyzed for the one-dimensional case in [9], it was further extended to higher dimensions in [28], and called MsFEM. In a broad sense, multiscale methods make the basis functions responsible for upscaling unresolved structures due to the use of coarse meshes. Local problems based on the original operator drive the basis functions and are completely independent of one another. The degrees of freedom are computed from a global problem posed on a coarse mesh. As a result, the multiscale method carries the "divide and conquer" approach found in domain decomposition methods. Other upscaling strategies produce different methods, such as the heterogenous multiscale method (HMM) [18], the localizable orthogonal decomposition (LOD) [32], the residual-free bubble (RFB) [13, 35] and the variational multiscale method (VMS) [29, 30], the subgrid finite element method (UpFEM) [6] and the generalized multiscale finite element method (GMsFEM) [19], just to cite a few. It has been only recently that multiscale finite element methods have been devised for the Stokes and Brinkman problems [1, 22, 3].

The hybridization technique can be an attractive alternative to tackle extreme-scale computations when combined with multiscale methods. Indeed, the hybridization strategy relies on decomposing the original model in local independent problems, which can be computed in parallel, by relaxing the continuity of variables and weakly imposing it through the adoption of Lagrange multipliers [34, 2, 15, 14]. As such, it is intrinsically related to the (vast) domain decomposition methodology. Also, it has been used, at the discrete level, to drive the construction of numerical method as the discontinuous enriched method (DEM) [21], or as a strategy to decrease the computational cost involved in the resolution of saddle-point problems. The latter viewpoint, first introduced in [8], has been recently revisited within the discontinuous Galerkin (DG) framework producing the hybrid discontinuous Galerkin (HDG) method [16]. Nevertheless,

the aforementioned hybridization approaches have only recently incorporated multiscale features of the media into their construction [20, 36, 7].

Combining the multiscale approach and the original hybrid concept presented in [34], we introduced in [25] a family of multiscale finite element method, named multiscale mixed-hybrid (MHM) method, for the second-order Darcy equation. The MHM method is a byproduct of the primal hybridization adopted at the continuous level. This is a fundamental difference with the HDG methodology. It was further analyzed in [4, 33], and extended to the reactive-advective dominated problem in [26] and to the linear elasticity in [24]. Also, an abstract setting was proposed in [31] and generalized in [27]. In this work, we extend the MHM method for Stokes and Brinkman models. Unlike previous works, the starting point is the dual hybrid formulation of the original model. Consequently, we recall first the procedure and prove that it does not change the original problem. In the sequel, we propose an equivalent (coupled) global-local formulation that characterizes the exact velocity and pressure variables in terms of piecewise constant functions and the Lagrange multipliers and the source term. This corresponds, indeed, to a new way of looking at the exact solutions and, consequently, it leads to a new MHM method.

We introduce the one-level version of the MHM method by choosing continuous (and discontinuous) polynomial interpolation spaces for the Lagrange multiplier on faces. In this case, one assumes that a closed formula for the multiscale basis functions is available. Although this may be seen as an unrealistic assumption in general, this first step is fundamental for the construction of an effective two-level MHM method presented next. There are a great deal of choices at the second level of discretization. Any stable or stabilized finite element method (or even other families of numerical methods) can be used, for instance, as long as they show approximation properties. In this work, we adopt the unusual stabilized finite element (USFEM) method originally proposed in [10]. The USFEM allows the use of equal-order pairs of interpolation spaces for the pressure and the velocity, is optimally convergent, and is robust with respect to vanishing diffusion. In summary, the MHM method proposed in this work has the following properties:

- precise on coarse meshes through upscaling;
- optimal, high-order convergent for the primal and dual variables;
- locally conservative;
- equal-order interpolations for all variables;
- adapted to extreme-scale parallel computing through a "divide and conquer" strategy;
- handles interfaces and boundary layers on not-aligned meshes;
- incorporate well-known finite element methods at the second-level and inherit their properties.

In addition to providing the construction of the method, the present work focuses on validating the MHM method through extensive numerical tests on a wide range of asymptotic regimes and heterogeneous coefficients. As such, the numerical analysis of the method is left to be addressed in a future work [5]. The outline of this paper is the following: this section ends with some notation and preliminary results. The one- and two-level MHM method are presented in Section 2, and validated numerically in Section 3. Conclusions are drawn in Section 4, with proofs of fundamental results in the appendix.

1.1. Notation and preliminaries

We introduce a regular family $\{\mathcal{T}_H\}_{H>0}$ of triangulations of $\overline{\Omega}$ into elements K, with diameter H_K and we set $H := \max_{K\in\mathcal{T}_H} H_K$. Hereafter, we shall use the terminology usually employed for three-dimensional domains, with the restriction to two-dimensional problems being straightforward. To each face F of $\mathcal{T}_H$, we associate a normal $\boldsymbol{n}$ taking care to ensure this is directed outward on $\partial\Omega$. We denote by $\mathcal{E}_H$ the set of all edges (faces) F of elements $K \in \mathcal{T}_H$. For each $K \in \mathcal{T}_H$ we further denote by $\boldsymbol{n}^K$ the outward normal on ∂K, and let $\boldsymbol{n}_F^K := \boldsymbol{n}^K|_F$ for each $F \subset \partial K$. On top of a partition $\mathcal{T}_H$, we define the spaces

$$\mathbf{V} = H^1(\mathcal{T}_H)^d := \{\boldsymbol{v} \in L^2(\Omega)^d \ : \ \boldsymbol{v}\,|_K \in H^1(K)^d \quad \text{for all } K \in \mathcal{T}_H\,\}, \tag{5}$$

$$\boldsymbol{\Lambda} := \left\{ \boldsymbol{\sigma}\, \boldsymbol{n}^K |_{\partial K} \in H^{-1/2}(\partial K)^d \quad \text{for all } K \in \mathcal{T}_H \,:\, \boldsymbol{\sigma} \in H(\text{div};\Omega) \right\}, \tag{6}$$

and $Q := L^2(\Omega)$, the spaces having their usual meaning. We define the inner product in $\mathbf{V}$

$$(\boldsymbol{u}, \boldsymbol{v})_{\mathbf{V}} := \frac{1}{d_\Omega^2}(\boldsymbol{u}, \boldsymbol{v})_\Omega + \sum_{K \in \mathcal{T}_H} (\nabla \boldsymbol{u}, \nabla \boldsymbol{v})_K \quad \text{for all } \boldsymbol{u},\, \boldsymbol{v} \in \mathbf{V}, \tag{7}$$

and we equip the spaces $H(\text{div};\Omega)$ for tensor variables and $\mathbf{V}$ with the norms, respectively,

$$\|\boldsymbol{\sigma}\|_{\text{div}}^2 := \sum_{K \in \mathcal{T}_H} \left(\|\boldsymbol{\sigma}\|_{0,K}^2 + d_\Omega^2 \, \|\nabla \cdot \boldsymbol{\sigma}\|_{0,K}^2 \right) \quad \text{and} \quad \|\boldsymbol{v}\|_{\mathbf{V}}^2 := \sum_{K \in \mathcal{T}_H} \left(d_\Omega^{-2} \, \|\boldsymbol{v}\|_{0,K}^2 + \|\nabla \boldsymbol{v}\|_{0,K}^2 \right), \tag{8}$$

where d_Ω is the diameter of Ω. As for the space $\boldsymbol{\Lambda}$, the quotient norm is used

$$\|\boldsymbol{\mu}\|_{\boldsymbol{\Lambda}} := \inf_{\substack{\boldsymbol{\sigma} \in H(\text{div};\Omega) \\ \boldsymbol{\sigma}\boldsymbol{n}^K = \boldsymbol{\mu} \text{ on } \partial K,\, K \in \mathcal{T}_H}} \|\boldsymbol{\sigma}\|_{\text{div}}. \tag{9}$$

We recall from [4, Lemma 8.3] that the norm (9) is equivalent to a dual norm, namely,

$$\frac{\sqrt{2}}{2} \, \|\boldsymbol{\mu}\|_\Lambda \le \sup_{\boldsymbol{v} \in \mathbf{V}} \frac{(\boldsymbol{\mu}, \boldsymbol{v})_{\partial \mathcal{T}_H}}{\|\boldsymbol{v}\|_{\mathbf{V}}} \le \|\boldsymbol{\mu}\|_{\boldsymbol{\Lambda}} \quad \text{for all } \boldsymbol{\mu} \in \boldsymbol{\Lambda}, \tag{10}$$

where

$$(\boldsymbol{\mu}, \boldsymbol{v})_{\partial \mathcal{T}_H} := \sum_{K \in \mathcal{T}_H} \langle \boldsymbol{\mu}, \boldsymbol{v} \rangle_{\partial K},$$

with $\langle \boldsymbol{\mu}, \boldsymbol{v} \rangle_{\partial K}$ being the duality pairing $H^{-1/2}(\partial K)^d \times H^{1/2}(\partial K)^d$. Also, we denote

$$(\boldsymbol{u}, \boldsymbol{v})_{\mathcal{T}_H} := \sum_{K \in \mathcal{T}_H} (\boldsymbol{u}, \boldsymbol{v})_K.$$

Above and hereafter we lighten the notation and understand the supremum to be taken over sets excluding the zero function, even though this is not specifically indicated. Also, we update the notation $a(\cdot,\cdot)$ and $b(\cdot,\cdot)$ by extending them to the space $\mathbf{V}$ as follows

$$a(\boldsymbol{w}, \boldsymbol{v}) := \sum_{K \in \mathcal{T}_H} a_K(\boldsymbol{w}, \boldsymbol{v}) \quad \text{with} \quad a_K(\boldsymbol{w}, \boldsymbol{v}) := (\nu \, \nabla \boldsymbol{w}, \nabla \boldsymbol{v})_K + (\boldsymbol{\gamma}\, \boldsymbol{w}, \boldsymbol{v})_K, \tag{11}$$

and

$$b(\boldsymbol{v}, q) := \sum_{K \in \mathcal{T}_H} b_K(\boldsymbol{v}, q) \quad \text{with} \quad b_K(\boldsymbol{v}, q) := -(\nabla \cdot \boldsymbol{v}, q)_K, \tag{12}$$

for all $\boldsymbol{w},\, \boldsymbol{v} \in \mathbf{V}$ and $q \in Q$. The starting point consists of replacing (3) by its hybrid formulation counterpart, i.e., find $(\boldsymbol{u}, p, \boldsymbol{\lambda}, \rho) \in \mathbf{V} \times Q \times \boldsymbol{\Lambda} \times \mathbb{R}$ such that

$$\begin{cases} a(\boldsymbol{u}, \boldsymbol{v}) + b(\boldsymbol{v}, p) + (\boldsymbol{\lambda}, \boldsymbol{v})_{\partial \mathcal{T}_H} = (\boldsymbol{f},\, \boldsymbol{v})_{\mathcal{T}_H} \quad \text{for all } \boldsymbol{v} \in \mathbf{V}, \\ b(\boldsymbol{u}, q) + (\rho, q)_\Omega = 0 \quad \text{for all } q \in Q, \\ (\boldsymbol{\mu}, \boldsymbol{u})_{\partial \mathcal{T}_H} = (\boldsymbol{\mu}, \boldsymbol{g})_{\partial \Omega} \quad \text{for all } \boldsymbol{\mu} \in \boldsymbol{\Lambda}, \\ (\xi, p)_\Omega = 0 \quad \text{for all } \xi \in \mathbb{R}. \end{cases} \tag{13}$$

The next result ensures that, when (3) is replaced by (13), we do not change the target solution. Its proof is postponed to the appendix (see Theorem 6).

Theorem 1. *The function $(\boldsymbol{u}, p) \in H^1(\Omega)^d \times L_0^2(\Omega)$ is the unique solution of (3) if and only if $(\boldsymbol{u}, p, \boldsymbol{\lambda}, \rho) \in \mathbf{V} \times Q \times \boldsymbol{\Lambda} \times \mathbb{R}$ is the unique solution of (13). Moreover, it holds $\rho = 0$ and*

$$\boldsymbol{\lambda} = \boldsymbol{\sigma}\, \boldsymbol{n}^K |_{\partial K} \quad \textit{for all } K \in \mathcal{T}_H, \tag{14}$$

where $\boldsymbol{\sigma} := -\nu \nabla \boldsymbol{u} + p\, \mathbf{I}$, and $\mathbf{I}$ is the $d \times d$ identity tensor.

2. The MHM method

The basic idea behind the Multiscale Hybrid-Mixed approach is to take advantage of the local nature of problem (13) by decomposing the statement into independent local problems and a face-based global problem which ties everything together. We formalize this idea next and build the MHM method from it.

We shall need some definitions first. Let $\mathbf{V}_0 \subset \mathbf{V}$ be the (closed) nullspace with definition,

$$\mathbf{V}_0 := \{\boldsymbol{v} \in \mathbf{V} \,:\, a(\boldsymbol{v}, \boldsymbol{w}) = 0 \quad \text{for all } \boldsymbol{w} \in \mathbf{V}\}\,.$$

Observe that for the Stokes problem ($\boldsymbol{\gamma} = 0$),

$$\mathbf{V}_0 = \left\{\boldsymbol{v} \in \mathbf{V} \,:\, \boldsymbol{v}\,|_K \in \mathbb{P}_0(K)^d \text{ for all } \; K \in \mathcal{T}_H\right\},$$

where $\mathbb{P}_0(K)$ stands for the space of piecewise constants, and $\mathbf{V}_0 = \{\mathbf{0}\}$ otherwise. Consider the decomposition

$$\mathbf{V} \;=\; \mathbf{V}_0 \oplus \mathbf{V}_0^{\perp}, \tag{15}$$

where $\mathbf{V}_0^{\perp}$ stands for the orthogonal complement with respect to the inner-product $(\cdot,\cdot)_{\mathbf{V}}$. For the Stokes equations ($\boldsymbol{\gamma} = 0$) we have

$$\mathbf{V}_0^{\perp} = \left\{\boldsymbol{v} \in \mathbf{V} \,:\, \boldsymbol{v}\,|_K \in [H^1(K) \cap L^2_0(K)]^d \text{ for all } \; K \in \mathcal{T}_H\right\},$$

and $\mathbf{V}_0^{\perp} = \mathbf{V}$ otherwise. Owing to decomposition (15), an element $\boldsymbol{v} \in \mathbf{V}$ admits the expansion $\boldsymbol{v} \;=\; \boldsymbol{v}_0 + \boldsymbol{v}_0^{\perp}$ in terms of a unique $\boldsymbol{v}_0 \in \mathbf{V}_0$ and $\boldsymbol{v}_0^{\perp} \in \mathbf{V}_0^{\perp}$. Particularly, the solution $\boldsymbol{u} \in \mathbf{V}$ of the hybrid problem (13) reads

$$\boldsymbol{u} \;=\; \boldsymbol{u}_0 + \boldsymbol{u}_0^{\perp}, \tag{16}$$

and then hybrid formulation (13) is equivalently written as: Find $(\boldsymbol{u}_0, \boldsymbol{u}_0^{\perp}, p, \boldsymbol{\lambda}, \rho) \in \mathbf{V}_0 \times \mathbf{V}_0^{\perp} \times Q \times \boldsymbol{\Lambda} \times \mathbb{R}$ such that

$$\left\{\begin{array}{c} (\boldsymbol{\lambda}, \boldsymbol{v}_0)_{\partial\mathcal{T}_H} = (\boldsymbol{f},\, \boldsymbol{v}_0)_{\mathcal{T}_H} \quad \text{for all } \boldsymbol{v}_0 \in \mathbf{V}_0, \\ (\boldsymbol{\mu}, \boldsymbol{u}_0)_{\partial\mathcal{T}_H} + (\boldsymbol{\mu}, \boldsymbol{u}_0^{\perp})_{\partial\mathcal{T}_H} = (\boldsymbol{\mu}, \boldsymbol{g})_{\partial\Omega} \quad \text{for all } \boldsymbol{\mu} \in \boldsymbol{\Lambda}, \\ (\xi, p)_{\Omega} = 0 \quad \text{for all } \xi \in \mathbb{R}, \end{array}\right. \tag{17}$$

$$\left\{\begin{array}{c} a(\boldsymbol{u}_0^{\perp}, \boldsymbol{v}_0^{\perp}) + b(\boldsymbol{v}_0^{\perp}, p) + (\boldsymbol{\lambda}, \boldsymbol{v}_0^{\perp})_{\partial\mathcal{T}_H} = (\boldsymbol{f},\, \boldsymbol{v}_0^{\perp})_{\mathcal{T}_H} \quad \text{for all } \boldsymbol{v}_0^{\perp} \in \mathbf{V}_0^{\perp}, \\ b(\boldsymbol{u}_0^{\perp}, q) + (\rho, q)_{\Omega} = 0 \quad \text{for all } q \in Q\,, \end{array}\right. \tag{18}$$

where we used $a(\boldsymbol{u}, \boldsymbol{v}_0) = 0$ for all $\boldsymbol{v}_0 \in \mathbf{V}_0$.

Denote by $\mathbf{V}_0^{\perp}(K)$ and $Q(K)$ the spaces $\mathbf{V}_0^{\perp}$ and Q restricted to $K \in \mathcal{T}_H$, respectively. System (18) can be localized in each $K \in \mathcal{T}_H$ by testing (17)-(18) with $(\boldsymbol{v}_0, \boldsymbol{v}_0^{\perp}, q, \boldsymbol{\mu}, \xi) = (\mathbf{0}, \boldsymbol{v}_0^{\perp}\,|_K, q\,|_K, \mathbf{0}, 0)$. This gives us

$$\left\{\begin{array}{c} a_K(\boldsymbol{u}_0^{\perp}, \boldsymbol{v}_0^{\perp}) + b_K(\boldsymbol{v}_0^{\perp}, p) = -\langle \boldsymbol{\lambda}, \boldsymbol{v}_0^{\perp}\rangle_{\partial K} + (\boldsymbol{f},\, \boldsymbol{v}_0^{\perp})_K \quad \text{for all } \boldsymbol{v}_0^{\perp} \in \mathbf{V}_0^{\perp}(K), \\ b_K(\boldsymbol{u}_0^{\perp}, q) = -(\rho, q)_K \quad \text{for all } q \in Q(K). \end{array}\right. \tag{19}$$

Note that from (19), $(\boldsymbol{u}_0^{\perp}, p)$ can be computed once $\boldsymbol{\lambda}$, $\boldsymbol{f}$ and ρ are known. Owing to the linearity of problem (19), we can formally write

$$\boldsymbol{u}_0^{\perp} \;=\; \boldsymbol{u}^{\boldsymbol{\lambda}} + \boldsymbol{u}^{\boldsymbol{f}} + \boldsymbol{u}^{\rho} \quad \text{and} \quad p \;=\; p^{\boldsymbol{\lambda}} + p^{\boldsymbol{f}} + p^{\rho}, \tag{20}$$

where we postpone the definition of the above notation for a moment.

Next, testing $(\boldsymbol{v}_0, \boldsymbol{v}_0^{\perp}, q, \boldsymbol{\mu}, \xi) = (\boldsymbol{v}_0, \mathbf{0}, 0, \boldsymbol{\mu}, \xi)$ in (17)-(18) and using (20), the global problem (17) reads: Find $(\boldsymbol{u}_0, \boldsymbol{\lambda}, \rho) \in \mathbf{V}_0 \times \boldsymbol{\Lambda} \times \mathbb{R}$ such that

$$\left\{\begin{array}{c} (\boldsymbol{\lambda}, \boldsymbol{v}_0)_{\partial\mathcal{T}_H} = (\boldsymbol{f},\, \boldsymbol{v}_0)_{\mathcal{T}_H}, \\ (\boldsymbol{\mu}, \boldsymbol{u}_0)_{\partial\mathcal{T}_H} + (\boldsymbol{\mu}, \boldsymbol{u}^{\boldsymbol{\lambda}})_{\partial\mathcal{T}_H} + (\boldsymbol{\mu}, \boldsymbol{u}^{\rho})_{\partial\mathcal{T}_H} = (\boldsymbol{\mu}, \boldsymbol{g})_{\partial\Omega} - (\boldsymbol{\mu}, \boldsymbol{u}^{\boldsymbol{f}})_{\partial\mathcal{T}_H}, \\ (\xi, p^{\boldsymbol{\lambda}})_{\Omega} + (\xi, p^{\rho})_{\Omega} = -(\xi, p^{\boldsymbol{f}})_{\Omega}, \end{array}\right. \tag{21}$$

for all $\boldsymbol{v}_0 \in \mathbf{V}_0$, $\boldsymbol{\mu} \in \boldsymbol{\Lambda}$ and $\xi \in \mathbb{R}$. The functions used in (20) and (21) are given as follows:

- $(\boldsymbol{u}^{\boldsymbol{\lambda}}, p^{\boldsymbol{\lambda}}) \in \mathbf{V}_0^{\perp} \times Q$ such that $\boldsymbol{u}^{\boldsymbol{\lambda}}|_K$ and $p^{\boldsymbol{\lambda}}|_K$ satisfy

$$\begin{cases} a_K(\boldsymbol{u}^{\boldsymbol{\lambda}}, \boldsymbol{w}) + b_K(\boldsymbol{w}, p^{\boldsymbol{\lambda}}) = -\langle \boldsymbol{\lambda}, \boldsymbol{w} \rangle_{\partial K} \quad \text{for all } \boldsymbol{w} \in \mathbf{V}_0^{\perp}(K), \\ b_K(\boldsymbol{u}^{\boldsymbol{\lambda}}, q) = 0 \quad \text{for all } q \in Q(K); \end{cases} \tag{22}$$

- $(\boldsymbol{u}^{\boldsymbol{f}}, p^{\boldsymbol{f}}) \in \mathbf{V}_0^{\perp} \times Q$ such that $\boldsymbol{u}^{\boldsymbol{f}}|_K$ and $p^{\boldsymbol{f}}|_K$ satisfy

$$\begin{cases} a_K(\boldsymbol{u}^{\boldsymbol{f}}, \boldsymbol{w}) + b_K(\boldsymbol{w}, p^{\boldsymbol{f}}) = (\boldsymbol{f}, \boldsymbol{w})_K \quad \text{for all } \boldsymbol{w} \in \mathbf{V}_0^{\perp}(K), \\ b_K(\boldsymbol{u}^{\boldsymbol{f}}, q) = 0 \quad \text{for all } q \in Q(K); \end{cases} \tag{23}$$

- $(\boldsymbol{u}^{\rho}, p^{\rho}) \in \mathbf{V}_0^{\perp} \times Q$ such that $\boldsymbol{u}^{\rho}|_K$ and $p^{\rho}|_K$ satisfy

$$\begin{cases} a_K(\boldsymbol{u}^{\rho}, \boldsymbol{w}) + b_K(\boldsymbol{w}, p^{\rho}) = 0 \quad \text{for all } \boldsymbol{w} \in \mathbf{V}_0^{\perp}(K), \\ b_K(\boldsymbol{u}^{\rho}, q) = -(\rho, q)_K \quad \text{for all } q \in Q(K). \end{cases} \tag{24}$$

It is worth mentioning that the dual variable

$$\boldsymbol{\sigma} := -\nu \nabla \boldsymbol{u}_0^{\perp} + p\,\mathbf{I},$$

belongs to the space $H(\mathrm{div};\Omega)$ since $\boldsymbol{\sigma}\,\boldsymbol{n}|_F$ is continuous across $F \in \mathcal{E}_h$ and $\boldsymbol{f} \in L^2(\Omega)^d$ by assumption [11, page 95]. The coupled global-local problem (21)–(24) is equivalent to the hybrid formulation (13), as indicated in the next result, whose proof is postponed to the appendix (see Theorem 7).

Theorem 2. *Consider $\boldsymbol{f} \in L^2(\Omega)^d$ and $\boldsymbol{g} \in H^{1/2}(\partial\Omega)^d$ with $\int_{\partial\Omega} \boldsymbol{g} \cdot \boldsymbol{n}\, ds = 0$. Problem (13) admits a unique solution $(\boldsymbol{u}, p, \boldsymbol{\lambda}, 0) \in \mathbf{V} \times Q \times \boldsymbol{\Lambda} \times \mathbb{R}$ if and only if problem (21) admits a unique solution $(\boldsymbol{u}_0, \boldsymbol{\lambda}, 0) \in \mathbf{V}_0 \times \boldsymbol{\Lambda} \times \mathbb{R}$. Moreover, the following characterizations hold:*

$$\boldsymbol{u} = \boldsymbol{u}_0 + \boldsymbol{u}^{\boldsymbol{\lambda}} + \boldsymbol{u}^{\boldsymbol{f}} \quad \textit{and} \quad p = p^{\boldsymbol{\lambda}} + p^{\boldsymbol{f}}. \tag{25}$$

2.1. The one-level MHM method

The MHM strategy, given by the coupled problems (21)–(24), is defined at the continuous level. We now head to its discretization, starting with its one-level version. This is accomplished by considering a finite dimensional space $\boldsymbol{\Lambda}_H$ of $\boldsymbol{\Lambda}$ such that

$$\boldsymbol{\Lambda}_0 \subseteq \boldsymbol{\Lambda}_H \subset \boldsymbol{\Lambda} \cap L^2(\mathcal{E}_H)^d, \tag{26}$$

with

$$\boldsymbol{\Lambda}_0 := \left\{ \boldsymbol{\sigma}\,\boldsymbol{n}^K|_F \in \mathbb{P}_0(F)^d \text{ for all } F \subset \partial K,\ K \in \mathcal{T}_H \,:\, \boldsymbol{\sigma} \in H(\mathrm{div};\Omega) \right\}, \tag{27}$$

where $\mathbb{P}_0(F)$ is the space of constant polynomial functions on F. The condition $\boldsymbol{\Lambda}_0 \subseteq \boldsymbol{\Lambda}_H$ is paramount, not only for decent approximation, but also to ensure the one-level MHM method is well-posed. Such a discussion is beyond the scope of the present work and will be addressed in [5]. We search for approximate Lagrange multipliers in the space spanned by piecewise polynomial functions, i.e.,

$$\boldsymbol{\Lambda}_H = \boldsymbol{\Lambda}_l^m := \left\{ \boldsymbol{\sigma}\,\boldsymbol{n}^K|_F \in \mathbb{P}_l^m(F)^d \text{ for all } F \subset \partial K,\ K \in \mathcal{T}_H \,:\, \boldsymbol{\sigma} \in H(\mathrm{div};\Omega) \right\}, \tag{28}$$

where $\mathbb{P}_l^m(F)$ is the space of discontinuous polynomial functions on F of degree less than or equal $l \geq 0$ and defined on an equally spaced partition of F, composed of m elements ($m \geq 1$). In what follows, the space $\boldsymbol{\Lambda}_l$ stands for $\boldsymbol{\Lambda}_l^1$. We illustrate in Figure 1 and Figure 2 an example of these spaces and the corresponding basis functions for the pressure and the velocity spaces.

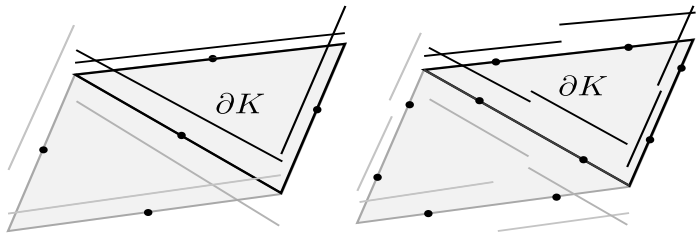

Figure 1: Difference between functions on a patch of two triangles elements belong to the space $\mathbf{\Lambda}_0$ (left) and $\mathbf{\Lambda}_0^2$ (right) [26].

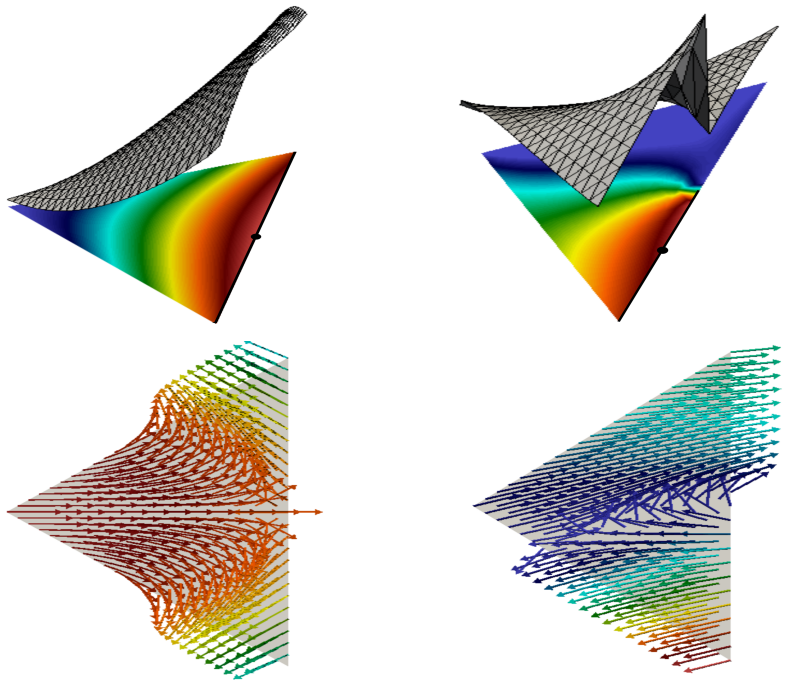

Figure 2: Example of basis functions using spaces $\mathbf{\Lambda}_0$ (left) and $\mathbf{\Lambda}_0^2$ (right). Pressure is shown at the top, and the velocity field at the bottom. We observe the impact of discontinuous interpolations for the Lagrange multipliers on the basis functions.

Unlike the usual interpolation choice [34], the functions in $\mathbf{\Lambda}_H$ may be discontinuous on faces $F \in \mathcal{E}_H$. Such a choice preserves the conformity of the MHM method and turns out to be central to maintaining the quality of the approximation when coefficients jump across faces. This will be explored in the numerical section. Specifically, the solution of (21) is approximated by $(\boldsymbol{u}_0^H, \boldsymbol{\lambda}_H, \rho_H) \in \mathbf{V}_0 \times \mathbf{\Lambda}_H \times \mathbb{R}$, which is the solution to the one-level MHM method

$$\left\{\begin{array}{c} (\boldsymbol{\lambda}_H, \boldsymbol{v}_0)_{\partial\mathcal{T}_H} = (\boldsymbol{f}, \boldsymbol{v}_0)_{\mathcal{T}_H}, \\ (\boldsymbol{\mu}_H, \boldsymbol{u}_0^H)_{\partial\mathcal{T}_H} + (\boldsymbol{\mu}_H, \boldsymbol{u}^{\boldsymbol{\lambda}_H})_{\partial\mathcal{T}_H} + (\boldsymbol{\mu}_H, \boldsymbol{u}^{\rho_H})_{\partial\mathcal{T}_H} = (\boldsymbol{\mu}_H, \boldsymbol{g})_{\partial\Omega} - (\boldsymbol{\mu}_H, \boldsymbol{u}^{\boldsymbol{f}})_{\partial\mathcal{T}_H}, \\ (\xi_H, p^{\boldsymbol{\lambda}_H})_\Omega + (\xi_H, p^{\rho_H})_\Omega = -(\xi_H, p^{\boldsymbol{f}})_\Omega, \end{array}\right. \tag{29}$$

for all $\boldsymbol{v}_0 \in \mathbf{V}_0$, $\boldsymbol{\mu}_H \in \mathbf{\Lambda}_H$ and $\xi_H \in \mathbb{R}$. Here we use the local problems (22)–(24) to compute velocities $\boldsymbol{u}^{\boldsymbol{\lambda}_H}$, $\boldsymbol{u}^{\boldsymbol{f}}$, $\boldsymbol{u}^{\rho_H}$ and pressures $p^{\boldsymbol{\lambda}_H}$, $p^{\boldsymbol{f}}$, p^{ρ_H}. Thus, the discrete solution $(\boldsymbol{u}_H, p_H)$ is given through the expressions

$$\boldsymbol{u}_H := \boldsymbol{u}_0^H + \boldsymbol{u}^{\boldsymbol{\lambda}_H} + \boldsymbol{u}^{\boldsymbol{f}} + \boldsymbol{u}^{\rho_H} \quad \text{and} \quad p_H := p^{\boldsymbol{\lambda}_H} + p^{\boldsymbol{f}} + p^{\rho_H}, \tag{30}$$

and then, the MHM method is not $H^1(\Omega)^d-$conforming. Nevertheless, there is a discrete stress tensor $\boldsymbol{\sigma}_H$, given by

$$\boldsymbol{\sigma}_H := -\nu\nabla\boldsymbol{u}_H + p_H\mathbf{I},$$

which is in $H(\mathrm{div};\Omega)$ because $\boldsymbol{\sigma}_H\,\boldsymbol{n}^K|_{\partial K} \in \boldsymbol{\Lambda}_H$ for all $K \in \mathcal{T}_H$. Also, the discrete stress tensor $\boldsymbol{\sigma}_H$ is automatically in equilibrium in each element $K \in \mathcal{T}_H$, i.e.,

$$\int_{\partial K} \boldsymbol{\sigma}_H\,\boldsymbol{n}^K\,d\mathbf{s} = \int_{\partial K} \boldsymbol{\lambda}_H\,d\mathbf{s} = \int_K \boldsymbol{f}\,d\boldsymbol{x},$$

where we used the first equation in (29). In any case, replacing $\boldsymbol{\Lambda}$ by $\boldsymbol{\Lambda}_H$ allows solutions to (22) and (24) to be found in terms of basis functions and gives rise to the one-level MHM method in (29). Here, we assume that the corresponding local problems are computed exactly, i.e, a closed formula for the multiscale basis functions is available.

Remark 1. *Discretization decouples the local problems* (22)–(24) *from the global one* (29)*. Thereby, a staggered algorithm can be adopted to solve the system. To see this more clearly, it is instructive to consider* $\boldsymbol{u}^{\boldsymbol{\lambda}_H}$ *and* $p^{\boldsymbol{\lambda}_H}$ *in more detail. First, suppose that* $\{\boldsymbol{\psi}_i\}_{i=1}^{\dim\boldsymbol{\Lambda}_H}$ *is a basis for* $\boldsymbol{\Lambda}_H$*, and define the sets* $\{\boldsymbol{\eta}_i^{\boldsymbol{u}}\}_{i=1}^{\dim\boldsymbol{\Lambda}_H} \subset \mathbf{V}_0^{\perp}$ *and* $\{\eta_i^p\}_{i=1}^{\dim\boldsymbol{\Lambda}_H} \subset Q$*, such that,*

$$\begin{cases} a_K(\boldsymbol{\eta}_i^{\boldsymbol{u}},\,\boldsymbol{w}) + b_K(\boldsymbol{w},\eta_i^p) = -\langle\boldsymbol{\psi}_i,\boldsymbol{w}\rangle_{\partial K} \quad \textit{for all } \boldsymbol{w} \in \mathbf{V}_0^{\perp}(K), \\ \qquad\qquad b_K(\boldsymbol{\eta}_i^{\boldsymbol{u}},q) = 0 \quad \textit{for all } q \in Q(K), \end{cases} \tag{31}$$

where $\boldsymbol{\psi}_i$ *changes its sign according to* $\boldsymbol{n}\cdot\boldsymbol{n}^K$ *on each* $F \subset \partial K$*. Now, supposing* $\boldsymbol{\lambda}_H = \sum_{i=1}^{\dim\boldsymbol{\Lambda}_H}\lambda_i\,\boldsymbol{\psi}_i$ *in* $\boldsymbol{\Lambda}_H$ *with* $\lambda_i \in \mathbb{R}$*, we observe that the linearity of problem* (22) *implies that we may uniquely write*

$$\boldsymbol{u}^{\boldsymbol{\lambda}_H} = \sum_{i=1}^{\dim\boldsymbol{\Lambda}_H}\lambda_i\,\boldsymbol{\eta}_i^{\boldsymbol{u}} \qquad \textit{and} \qquad p^{\boldsymbol{\lambda}_H} = \sum_{i=1}^{\dim\boldsymbol{\Lambda}_H}\lambda_i\,\eta_i^p.$$

Therefore, the degrees of freedom λ_i *of* $\boldsymbol{\lambda}_H$ *are "inherited" by* $\boldsymbol{u}^{\boldsymbol{\lambda}_H}$ *and* $p^{\boldsymbol{\lambda}_H}$*. As a result, the global formulation* (29) *is responsible for computing the degrees of freedom of* $\boldsymbol{u}_0$ *(d per element) and* λ_i*, once the multiscale basis functions* $(\boldsymbol{\eta}_i^{\boldsymbol{u}},\eta_i^p)$ *and* $(\boldsymbol{u}^{\boldsymbol{f}},p^{\boldsymbol{f}})$ *are available from the local problems. Also, it is interesting to note that heterogeneous and/or high-contrast aspects of the media automatically impact the design of the basis functions* $(\boldsymbol{\eta}_i^{\boldsymbol{u}},\eta_i^p)$ *as well as* $(\boldsymbol{u}^{\boldsymbol{f}},p^{\boldsymbol{f}})$*, as they are driven by the local problems* (31) *and* (23)*, respectively. Similarly, let* $\rho_H = \rho_0\,1_\Omega$ *where* $\rho_0 \in \mathbb{R}$*. Then, we can write*

$$\boldsymbol{u}^{\rho_H} = \rho_0\,\boldsymbol{\chi}^{\boldsymbol{u}} \quad \textit{and} \quad p^{\rho_H} = \rho_0\,\chi^p,$$

where, in each $K \in \mathcal{T}_H$*,* $(\boldsymbol{\chi}^{\boldsymbol{u}},\chi^p)$ *satisfies*

$$\begin{cases} a_K(\boldsymbol{\chi}^{\boldsymbol{u}},\,\boldsymbol{w}) + b_K(\boldsymbol{w},\chi^p) = 0 \quad \textit{for all } \boldsymbol{w} \in \mathbf{V}_0^{\perp}(K), \\ \qquad\qquad b_K(\boldsymbol{\chi}^{\boldsymbol{u}},q) = (1_\Omega,q)_K \quad \textit{for all } q \in Q(K). \end{cases} \tag{32}$$

Observe $(\boldsymbol{\chi}^{\boldsymbol{u}},\chi^p)$ *would also be available by solving a global problem driven by the function* 1_Ω*. Here, we decide to obtain it from* (32) *to keep computations local.*

Remark 2. *Following the ideas of Theorem 2, we can prove that* $\boldsymbol{u}^{\rho_H} = \mathbf{0}$ *and* $p^{\rho_H} = 0$*, and then, the discrete solution* (30) *is reduced to*

$$\boldsymbol{u}_H := \boldsymbol{u}_0^H + \boldsymbol{u}^{\boldsymbol{\lambda}_H} + \boldsymbol{u}^{\boldsymbol{f}} \quad \textit{and} \quad p_H := p^{\boldsymbol{\lambda}_H} + p^{\boldsymbol{f}}.$$

In fact, using local problems (22)–(24)*, with* $q = 1_K$ *and* $\boldsymbol{w} = \mathbf{0}$*, we get*

$$\int_K \nabla\cdot\boldsymbol{u}_H\,d\boldsymbol{x} = \int_K \rho_H\,d\boldsymbol{x} = \rho_H|K|, \tag{33}$$

for each $K \in \mathcal{T}_H$. Furthermore, we use (29) *to arrive at*

$$(\boldsymbol{\mu}_H, \boldsymbol{u}_H)_{\partial\mathcal{T}_H} = (\boldsymbol{\mu}_H, \boldsymbol{g})_{\partial\Omega} \quad \text{for all } \boldsymbol{\mu}_H \in \boldsymbol{\Lambda}_H. \tag{34}$$

Now, take $\boldsymbol{\sigma}^* := \rho_H \mathbf{I}$. It is clear that $\boldsymbol{\sigma}^* \in H(\mathrm{div};\Omega)$, and thus, $\boldsymbol{\mu}^* := \boldsymbol{\sigma}^* \boldsymbol{n}^K|_{\partial K} \in \boldsymbol{\Lambda}_H$ for each $K \in \mathcal{T}_H$ since $\boldsymbol{\Lambda}_0 \subset \boldsymbol{\Lambda}_H$. As a result, testing $\boldsymbol{\mu}^*$ in (34) *and from* (33)*, it holds*

$$|\Omega|\, \rho_H^2 = \sum_{K\in\mathcal{T}_H} \rho_H \int_{\partial K} \boldsymbol{u}_H \cdot \boldsymbol{n}^K \, d\boldsymbol{s} = \rho_H \int_{\partial\Omega} \boldsymbol{g} \cdot \boldsymbol{n} \, d\boldsymbol{s}\,. \tag{35}$$

Hence, from the compatibility condition $\int_{\partial\Omega} \boldsymbol{g} \cdot \boldsymbol{n}\, d\boldsymbol{s} = 0$, we arrive at $\rho_H = 0$ and the result follows from (24)*.*

2.2. The two-level MHM method

Although in some cases the basis $\{(\boldsymbol{\eta}_i^{\boldsymbol{u}}, \eta_i^p)\}_{i=1}^{\dim \boldsymbol{\Lambda}_H}$ and $(\boldsymbol{u}^{\boldsymbol{f}}, p^{\boldsymbol{f}})$ in Remark 1 are readily available for use in (29) (observe, for instance, that if $\boldsymbol{f} \in \mathbb{P}_0(K)^d$ then $\boldsymbol{u}^{\boldsymbol{f}}$ vanishes) the one-level MHM method is, in most cases, impractical. This is particularly true for more complex coefficients ν and/or $\boldsymbol{\gamma}$ (due to multiscale or high-contrast aspects) and for higher-order interpolation on faces. In these cases a two-level method is mandatory. This is the subject of this section.

It is interesting to note that the two-level MHM method may be quite general since it can embed a variety of local methods and/or interpolation spaces to approximate solutions to (22)–(24). For instance, the Galerkin method with a classical stable pair of finite element spaces [11] or a hybrid discontinuous Galerkin (HDG) method [17], just to cite a few, can be adopted as a second-level solver. One may even adopt different numerical methods in different elements. For sake of simplicity, we do not follow this option here since it would further overload the notation.

Here, we pursue the standard conforming approach. We begin by selecting local finite dimensional spaces $\mathbf{V}_h(K) \subset \mathbf{V}_0^{\perp}(K)$ and $Q_h(K) \subset Q(K)$ whose functions are defined over a regular partition of K, denoted by $\{\mathcal{T}_h^K\}_{h>0}$, where h is the characteristic length of $\mathcal{T}_h^K$. Particularly, hereafter we adopt the following nodal polynomial spaces

$$\mathbf{V}_h(K) := \left\{ \boldsymbol{v}_h \in \mathbf{V}_0^{\perp}(K) \cap C^0(K)^d \,:\, \boldsymbol{v}_h|_\tau \in \mathbb{P}_k(\tau)^d \text{ for all } \tau \in \mathcal{T}_h^K \right\}, \tag{36}$$

and

$$Q_h(K) := \left\{ q_h \in Q(K) \cap C^0(K) \,:\, q_h|_\tau \in \mathbb{P}_n(\tau) \text{ for all } \tau \in \mathcal{T}_h^K \right\}, \tag{37}$$

where $\mathbb{P}_s(\tau)$ is the polynomial space of functions in $\tau \in \mathcal{T}_h^K$ with total degree less than or equal to $s \geq 1$. Such a partition may differ in each $K \in \mathcal{T}_H$, as may the degree of polynomial functions. By setting the global finite dimensional spaces as

$$\mathbf{V}_h := \oplus_{K\in\mathcal{T}_H} \mathbf{V}_h(K) \quad \text{and} \quad Q_h := \oplus_{K\in\mathcal{T}_H} Q_h(K), \tag{38}$$

the two-level MHM method reads: Find $(\boldsymbol{u}_0^{H,h}, \boldsymbol{\lambda}_H, \rho_H) \in \mathbf{V}_0 \times \boldsymbol{\Lambda}_H \times \mathbb{R}$ such that

$$\left\{ \begin{array}{c} (\boldsymbol{\lambda}_H, \boldsymbol{v}_0)_{\partial\mathcal{T}_H} = (\boldsymbol{f},\, \boldsymbol{v}_0)_{\mathcal{T}_H}, \\ (\boldsymbol{\mu}_H, \boldsymbol{u}_0^{H,h})_{\partial\mathcal{T}_H} + (\boldsymbol{\mu}_H, \boldsymbol{u}_h^{\boldsymbol{\lambda}_H})_{\partial\mathcal{T}_H} + (\boldsymbol{\mu}_H, \boldsymbol{u}_h^{\rho_H})_{\partial\mathcal{T}_H} = (\boldsymbol{\mu}_H, \boldsymbol{g})_{\partial\Omega} - (\boldsymbol{\mu}_H, \boldsymbol{u}_h^{\boldsymbol{f}})_{\partial\mathcal{T}_H}, \\ (\xi_H, p_h^{\boldsymbol{\lambda}_H})_\Omega + (\xi_H, p_h^{\rho_H})_\Omega = -(\xi_H, p_h^{\boldsymbol{f}})_\Omega, \end{array} \right. \tag{39}$$

for all $(\boldsymbol{v}_0, \boldsymbol{\mu}_H, \xi_H) \in \mathbf{V}_0 \times \boldsymbol{\Lambda}_H \times \mathbb{R}$. The appealing option of using equal-order nodal pairs of interpolation spaces for the velocity and the pressure variables (i.e. $k = n$ in (36) and (37)) is made available by adopting the unusual stabilized finite element method (USFEM) proposed in [10] as the second-level solver. For

completeness, we recall (see [10] for details) that the USFEM consists of finding $(\boldsymbol{u}, p) \in \mathbf{V}_h(K) \times Q_h(K)$ such that

$$B_K(\boldsymbol{u}, p; \boldsymbol{v}, q) = F_K(\boldsymbol{v}, q) \quad \text{for all } (\boldsymbol{v}, q) \in \mathbf{V}_h(K) \times Q_h(K), \tag{40}$$

where

$$B_K(\boldsymbol{u}, p; \boldsymbol{v}, q) := a_K(\boldsymbol{u}, \boldsymbol{v}) + b_K(\boldsymbol{v}, p) - b_K(\boldsymbol{u}, q) - \sum_{\tau \in \mathcal{T}_h^K} \kappa_\tau(-\nu \Delta \boldsymbol{u} + \boldsymbol{\gamma}\, \boldsymbol{u} + \nabla p, -\nu \Delta \boldsymbol{v} + \boldsymbol{\gamma}\, \boldsymbol{v} - \nabla q)_\tau, \tag{41}$$

and

$$F_K(\boldsymbol{v}, q) := (\boldsymbol{f}, \boldsymbol{v})_K - \sum_{\tau \in \mathcal{T}_h^K} \kappa_\tau(\boldsymbol{f}, -\nu \Delta \boldsymbol{v} + \boldsymbol{\gamma}\, \boldsymbol{v} - \nabla q)_\tau. \tag{42}$$

The so-called stabilization parameter is given by

$$\kappa_\tau := \frac{h_\tau^2}{\boldsymbol{\gamma}_{\min} h_\tau^2 \, \max\{1, Pe_\tau\} + \frac{4\,\nu}{m_\tau}} \qquad \text{and} \qquad Pe_\tau := \frac{4\,\nu}{\boldsymbol{\gamma}_{\min}\, h_\tau^2\, m_\tau},$$

where $\boldsymbol{\gamma}_{\min}$ is the minimum eigenvalue of $\boldsymbol{\gamma}$, $m_\tau = \min\left\{\frac{1}{3}, C_\tau\right\}$, and

$$C_\tau\, h_\tau^2\, \|\Delta \boldsymbol{v}\|_{0,\tau}^2 \leq \|\nabla \boldsymbol{v}\|_{0,\tau}^2 \quad \text{for all } \boldsymbol{v} \in \mathbf{V}_h(K).$$

Owing to definition (40), the local solutions in (22)-(24) are approximated, in each $K \in \mathcal{T}_H$, by the solutions of the following stabilized methods:

- Find $(\boldsymbol{u}_h^{\boldsymbol{\lambda}_H}, p_h^{\boldsymbol{\lambda}_H}) \in \mathbf{V}_h \times Q_h$ such that

$$B_K(\boldsymbol{u}_h^{\boldsymbol{\lambda}_H}, p_h^{\boldsymbol{\lambda}_H}; \boldsymbol{v}_h, q_h) = -\langle \boldsymbol{\lambda}_H, \boldsymbol{v}_h \rangle_{\partial K} \quad \text{for all } (\boldsymbol{v}_h, q_h) \in \mathbf{V}_h(K) \times Q_h(K); \tag{43}$$

- Find $(\boldsymbol{u}_h^{\boldsymbol{f}}, p_h^{\boldsymbol{f}}) \in \mathbf{V}_h \times Q_h$ such that

$$B_K(\boldsymbol{u}_h^{\boldsymbol{f}}, p_h^{\boldsymbol{f}}; \boldsymbol{v}_h, q_h) = F_K(\boldsymbol{v}_h, q_h) \quad \text{for all } (\boldsymbol{v}_h, q_h) \in \mathbf{V}_h(K) \times Q_h(K); \tag{44}$$

- Find $(\boldsymbol{u}_h^{\rho_H}, p_h^{\rho_H}) \in \mathbf{V}_h \times Q_h$ such that

$$B_K(\boldsymbol{u}_h^{\rho_H}, p_h^{\rho_H}; \boldsymbol{v}_h, q_h) = (\rho_H, q_h)_K \quad \text{for all } (\boldsymbol{v}_h, q_h) \in \mathbf{V}_h(K) \times Q_h(K). \tag{45}$$

Remark 3. *From [10], the second-level approximate solutions $(\boldsymbol{u}_h^{\boldsymbol{\lambda}_H}, p_h^{\boldsymbol{\lambda}_H})$, $(\boldsymbol{u}_h^{\boldsymbol{f}}, p_h^{\boldsymbol{f}})$ and $(\boldsymbol{u}_h^{\rho_H}, p_h^{\rho_H})$ converge with optimal rate toward $(\boldsymbol{u}^{\boldsymbol{\lambda}_H}, p^{\boldsymbol{\lambda}_H})$, $(\boldsymbol{u}^{\boldsymbol{f}}, p^{\boldsymbol{f}})$ and $(\boldsymbol{u}^{\rho_H}, p^{\rho_H})$, respectively, as h goes to zero. Observe that, as is shown in Remark 2, we get $\rho_H = 0$ and then $\boldsymbol{u}_h^{\rho_H} = \mathbf{0}$ and $p_h^{\rho_H} = 0$. As a result, the discrete two-level solution $(\boldsymbol{u}_{H,h}, p_{H,h})$ is given through the expressions*

$$\boldsymbol{u}_{H,h} := \boldsymbol{u}_0^{H,h} + \boldsymbol{u}_h^{\boldsymbol{\lambda}_H} + \boldsymbol{u}_h^{\boldsymbol{f}} \quad \textit{and} \quad p_{H,h} := p_h^{\boldsymbol{\lambda}_H} + p_h^{\boldsymbol{f}}. \tag{46}$$

On the other hand, testing problems (43) and (44) with $(\boldsymbol{v}_h, q_h) = (\mathbf{0}, 1_K) \in \mathbf{V}_h(K) \times Q_h(K)$ and using $\rho_H = 0$, we have that the velocity field $\boldsymbol{u}_{H,h}$ in (46) conserves mass locally, i.e.,

$$\int_K \nabla \cdot \boldsymbol{u}_{H,h}\, d\boldsymbol{x} = 0 \quad \textit{for all } K \in \mathcal{T}_H. \tag{47}$$

Well-posedness for the two-level MHM method (39) relies on a compatibility condition between the space for the Lagrange multipliers $\boldsymbol{\Lambda}_H$ in (28) and the space for the velocity space $\mathbf{V}_h$ (which, in turn, is related to the pressure space Q_h). Applying the abstract setting introduced in [27], and under condition (26), the two-level MHM method (39) has a unique solution if and only if the following condition holds:

$$\{\boldsymbol{\mu}_H \in \boldsymbol{\Lambda}_H \,:\, (\boldsymbol{\mu}_H, \boldsymbol{v}_h)_{\partial\mathcal{T}_H} = 0 \quad \text{for all } \boldsymbol{v}_h \in \mathbf{V}_h\} = \{\mathbf{0}\}. \tag{48}$$

Condition (48) guarantees that the mapping $\boldsymbol{\mu}_H \mapsto (\boldsymbol{u}_h^{\boldsymbol{\mu}_H}, p_h^{\boldsymbol{\mu}_H})$ is injective, where $(\boldsymbol{u}_h^{\boldsymbol{\mu}_H}, p_h^{\boldsymbol{\mu}_H})$ solves (43). Such a property is central to proof that the bilinear form $(\boldsymbol{\mu}_H, \boldsymbol{u}_h^{\boldsymbol{\lambda}_H})_{\partial\mathcal{T}_H}$ in (39) is $\inf-\sup$ stable, which is one of the conditions in [27, Lemma 3] to prove the well-posedness of (39). The other conditions in [27, Lemma 3] are fulfilled using (26). The details are out of the scope of this work, and are addressed in [5].

Here, we employ condition (48) as a roadmap to chose $\mathbf{V}_h \times Q_h$ with respect to the space $\boldsymbol{\Lambda}_H$ in (28). As such, we fix $m = 1$ and highlight the relationship between l (the degree of polynomials in $\boldsymbol{\Lambda}_l$) and k (the degree of polynomials in $\mathbf{V}_h$) such that (48) holds in the case of a single element sub-mesh. This is the subject of the next lemma.

Lemma 3. *Assume that the second level mesh $\mathcal{T}_h^K$ is composed of a single element for all $K \in \mathcal{T}_H$. Then, condition* (48) *holds in*

(i) the 2D case if and only if

$$k \geq \begin{cases} l+1 & \text{when } l \text{ is even,} \\ l+2 & \text{when } l \text{ is odd;} \end{cases} \tag{49}$$

(ii) the 3D case if $k \geq l+3$.

Proof. Item (i) follows from Lemma 4 and Theorem 2 in [34], and item (ii) from [23] (see [5] for details).

Remark 4. *Sub-meshes are mandatory when highly heterogeneous coefficients of the media still persist in the interior of the coarse mesh elements. This scenario is most likely to occur since global coarse meshes must be used. It is important to verify when condition* (48) *holds. Clearly,* (48) *is verified if piecewise continuous interpolations fulfill the conditions in Lemma 3. Also, we verify numerically in Section 3.2 that the case $k = l$ for the velocity and the pressure works provided a "sufficiently" refined sub-mesh is used. This appealing option deserves further theoretical investigation.*

Remark 5. *By applying the viewpoint used in Remark 1 to the local problem* (43)*, the basis functions $(\boldsymbol{\eta}_i^{\boldsymbol{u}}, \eta_j^p)$ are approximated by $(\boldsymbol{\eta}_{i,h}^{\boldsymbol{u}}, \eta_{i,h}^p) \in \mathbf{V}_h(K) \times Q_h(K)$ in each $K \in \mathcal{T}_H$ as the solution of*

$$B_K(\boldsymbol{\eta}_{i,h}^{\boldsymbol{u}}, \eta_{i,h}^p; \boldsymbol{v}_h, q_h) = -\langle \boldsymbol{\psi}_i, \boldsymbol{v}_h \rangle_{\partial K} \quad \text{for all } (\boldsymbol{v}_h, q_h) \in \mathbf{V}_h(K) \times Q_h(K), \tag{50}$$

for all basis functions $\boldsymbol{\psi}_i \in \boldsymbol{\Lambda}_H$, with $i = 1, \ldots, \dim \boldsymbol{\Lambda}_H$. Assuming that the spaces $\mathbf{V}_h$ and $\boldsymbol{\Lambda}_H$ are such that the mapping $\boldsymbol{\psi}_i \mapsto (\boldsymbol{\eta}_{i,h}^{\boldsymbol{u}}, \eta_{i,h}^p)$ is injective, where $(\boldsymbol{\eta}_{i,h}^{\boldsymbol{u}}, \eta_{i,h}^p)$ solves (50)*, it follows that $\left\{\boldsymbol{\eta}_{i,h}^{\boldsymbol{u}}\right\}_{i=1}^{\dim \boldsymbol{\Lambda}_H}$ and $\left\{\eta_{i,h}^p\right\}_{i=1}^{\dim \boldsymbol{\Lambda}_H}$ generate proper subspaces of $\mathbf{V}_h$ and Q_h, respectively. Interestingly, if one assumes that a one element sub-mesh is used at the second level, the hybrid formulation* (13) *discretized using the space $\mathbf{V}_0 \oplus span\left\{\boldsymbol{\eta}_{i,h}^{\boldsymbol{u}} \,:\, i = 1, \ldots, \dim \boldsymbol{\Lambda}_H\right\}$ for the velocity and $span\left\{\eta_{i,h}^p \,:\, i = 1, \ldots, \dim \boldsymbol{\Lambda}_H\right\}$ for the pressure yield the same numerical solution as if we had solved the hybrid formulation with $\mathbf{V}_0 \oplus \mathbf{V}_h$ and Q_h for the velocity and the pressure, respectively. This is highlighted in Corollary 1 in [27] (see also Remark 3 in [27]). This viewpoint is related to the idea of minimally stable space proposed in [12].*

3. Numerical validations

We begin this section by providing the underlying algorithm for the MHM method (39). To this end, we define some notations first. Define the integer numbers

$$m_H := \text{card}(\mathcal{T}_H), \quad m_0 := \dim \mathbf{V}_0 = d \times m_H \qquad \text{and} \qquad m_\lambda := \dim \boldsymbol{\Lambda}_H.$$

Let $\{\boldsymbol{\psi}_1, \boldsymbol{\psi}_2, \ldots, \boldsymbol{\psi}_{m_\lambda}\}$ and $\{\boldsymbol{\phi}_1, \boldsymbol{\phi}_2, \ldots, \boldsymbol{\phi}_{m_0}\}$ be a basis for $\boldsymbol{\Lambda}_H$ and $\mathbf{V}_0$, respectively. Then, there exist real numbers $\lambda_1, \lambda_2, \ldots, \lambda_{m_\lambda}$ and $u_0^1, u_0^2, \ldots, u_0^{m_0}$, and ρ_0 such that

$$\boldsymbol{\lambda}_H = \sum_{i=1}^{m_\lambda} \lambda_i \, \boldsymbol{\psi}_i \quad \text{and} \quad \boldsymbol{u}_0^{H,h} = \sum_{i=1}^{m_0} u_0^i \, \boldsymbol{\phi}_i \quad \text{and} \quad \rho_H = \rho_0 \, 1_\Omega .$$

We can rewrite (39) as the linear system,

$$\begin{bmatrix} \mathcal{A} & \mathcal{B}^T & \mathcal{C}^T \\ \mathcal{B} & -\mathcal{D} & 0 \\ \mathcal{C} & \mathbf{0} & \mathbf{0} \end{bmatrix} \begin{bmatrix} \vec{\boldsymbol{\lambda}} \\ \rho_0 \\ \vec{\boldsymbol{u}}_0 \end{bmatrix} = \begin{bmatrix} \mathbf{F}_1 \\ F_2 \\ \mathbf{F}_3 \end{bmatrix}, \tag{51}$$

with $\vec{\boldsymbol{\lambda}}^T = (\lambda_1, \lambda_2, \ldots, \lambda_{m_\lambda}) \in \mathbb{R}^{m_\lambda}$ and $\vec{\boldsymbol{u}}_0^T = (u_0^1, u_0^2, \ldots, u_0^{m_0}) \in \mathbb{R}^{m_0}$. Note that the matrix in (51) has a size $(m_\lambda + m_0 + 1) \times (m_\lambda + m_0 + 1)$, and its components are given by

$$\begin{aligned}
&\mathcal{A} = (a_{ij}) \in \mathbb{R}^{m_\lambda \times m_\lambda} && \text{with} \quad a_{ij} := -(\boldsymbol{\psi}_i, \boldsymbol{\eta}_{j,h}^{\boldsymbol{u}})_{\partial \mathcal{T}_H}, \quad 1 \le i, j \le m_\lambda, \\
&\mathcal{B} = (b_{1j}) \in \mathbb{R}^{1 \times m_\lambda} && \text{with} \quad b_{1j} := -(\boldsymbol{\psi}_j, \boldsymbol{\chi}_h^{\boldsymbol{u}})_{\partial \mathcal{T}_H}, \quad 1 \le j \le m_\lambda , \\
&\mathcal{C} = (c_{ij}) \in \mathbb{R}^{m_0 \times m_\lambda} && \text{with} \quad c_{ij} := -(\boldsymbol{\psi}_j, \boldsymbol{\phi}_i)_{\partial \mathcal{T}_H}, \quad 1 \le i \le m_0 \quad \text{and} \quad 1 \le j \le m_\lambda , \\
&\mathcal{D} = (d) \in \mathbb{R} && \text{with} \quad d := (1_\Omega, \chi_h^p)_{\mathcal{T}_H} .
\end{aligned}$$

The entries of the global right hand side are

$$\begin{aligned}
&\mathbf{F}_1 = (f_i^1) \in \mathbb{R}^{m_\lambda} && \text{with} \quad f_i^1 := (\boldsymbol{\psi}_i, \boldsymbol{u}_h^{\boldsymbol{f}})_{\partial \mathcal{T}_H} - (\boldsymbol{\psi}_i, \boldsymbol{g})_{\partial \Omega}, \quad 1 \le i \le m_\lambda, \\
&F_2 = (f^2) \in \mathbb{R} && \text{with} \quad f^2 := (1_\Omega, \, p_h^{\boldsymbol{f}})_{\mathcal{T}_H} , \\
&\mathbf{F}_3 = (f_i^3) \in \mathbb{R}^{m_0} && \text{with} \quad f_i^3 := -(\boldsymbol{f}, \, \boldsymbol{\phi}_i)_{\mathcal{T}_H}, \quad 1 \le i \le m_0 .
\end{aligned}$$

We recall that $(\boldsymbol{\eta}_{j,h}^{\boldsymbol{u}}, \eta_{j,h}^p)$, $(\boldsymbol{u}_h^{\boldsymbol{f}}, p_h^{\boldsymbol{f}})$ and $(\boldsymbol{\chi}_h^{\boldsymbol{u}}, \chi_h^p)$ are the approximation of $(\boldsymbol{\eta}_j^{\boldsymbol{u}}, \eta_j^p)$, $(\boldsymbol{u}^{\boldsymbol{f}}, p^{\boldsymbol{f}})$ and $(\boldsymbol{\chi}^{\boldsymbol{u}}, \chi^p)$, defined locally as the solutions of the USFEM formulations: Find $(\boldsymbol{\eta}_{j,h}^{\boldsymbol{u}}, \eta_{j,h}^p) \in \mathbf{V}_h(K) \times Q_h(K)$ the solution of

$$B_K(\boldsymbol{\eta}_{j,h}^{\boldsymbol{u}}, \eta_{j,h}^p; \boldsymbol{v}_h, q_h) = -\langle \boldsymbol{\psi}_j, \boldsymbol{v}_h \rangle_{\partial K} \quad \text{for all } (\boldsymbol{v}_h, q_h) \in \mathbf{V}_h(K) \times Q_h(K) ,$$

and $(\boldsymbol{u}_h^{\boldsymbol{f}}, p_h^{\boldsymbol{f}}) \in \mathbf{V}_h(K) \times Q_h(K)$ the solution of

$$B_K(\boldsymbol{u}_h^{\boldsymbol{f}}, p_h^{\boldsymbol{f}}; \boldsymbol{v}_h, q_h) = F_K(\boldsymbol{v}_h, q_h) \quad \text{for all } (\boldsymbol{v}_h, q_h) \in \mathbf{V}_h(K) \times Q_h(K) ,$$

and $(\boldsymbol{\chi}_h^{\boldsymbol{u}}, \chi_h^p) \in \mathbf{V}_h(K) \times Q_h(K)$ the solution of

$$B_K(\boldsymbol{\chi}_h^{\boldsymbol{u}}, \chi_h^p; \boldsymbol{v}_h, q_h) = (1_\Omega, q_h)_K \quad \text{for all } (\boldsymbol{v}_h, q_h) \in \mathbf{V}_h(K) \times Q_h(K) .$$

Remark 6. *In the Stokes case ($\boldsymbol{\gamma} = \mathbf{0}$), a simple computation shows us that*

$$\boldsymbol{\chi}_h^{\boldsymbol{u}} = \frac{1}{d} \left(\mathbf{I} - \Pi_K \right) \boldsymbol{x} \quad \textit{and} \quad \chi_h^p = \frac{\nu}{d}, \tag{52}$$

where Π_K is the local L^2-projection onto $\mathbb{P}_0(K)^d$, for all $K \in \mathcal{T}_H$. In such a case, the matrix $\mathcal{D}$ is equal to $\frac{\nu}{d}|\Omega|$. Thereby, system (51) is reduced to

$$\begin{bmatrix} \tilde{\mathcal{A}} & \mathcal{C}^T \\ \mathcal{C} & \mathbf{0} \end{bmatrix} \begin{bmatrix} \vec{\boldsymbol{\lambda}} \\ \vec{\boldsymbol{u}}_0 \end{bmatrix} = \begin{bmatrix} \tilde{\mathbf{F}}_1 \\ \mathbf{F}_3 \end{bmatrix}, \tag{53}$$

where $\tilde{\mathcal{A}} := \mathcal{A} + \mathcal{B}^T \mathcal{D}^{-1} \mathcal{B}$ and $\tilde{\mathbf{F}}_1 := \mathbf{F}_1 + \mathcal{B}^T \mathcal{D}^{-1} F_2$. Note that in this case the computation of matrix $\mathcal{B}$ is also simplified thanks to the closed formula for $\boldsymbol{\chi}_h^{\boldsymbol{u}}$.

Next, we outline the algorithm for the Stokes case, noting that the Brinkman version follows from a straightforward modification. Let $\{\boldsymbol{\xi}_1^K, \boldsymbol{\xi}_2^K, \ldots, \boldsymbol{\xi}_{m_{h,K}}^K\}$, with $m_{h,K} := \dim \mathbf{V}_h(K)$, a basis of $\mathbf{V}_h(K)$ and $\{q_1^K, q_2^K, \ldots, q_{l_{h,K}}^K\}$, with $l_{h,K} := \dim Q_h(K)$, a basis of $Q_h(K)$, respectively. We define the following vectors and matrices:

$$\boldsymbol{S}_{j,K} := -\left(\langle \boldsymbol{\psi}_j, \boldsymbol{\xi}_k^K \rangle_{\partial K}\right)_k \in \mathbb{R}^{m_{h,K}} \quad 1 \leq j \leq m_\lambda \quad \text{and} \quad \boldsymbol{R}_K := \left(\left(1_\Omega, q_k^K\right)_K\right)_k \in \mathbb{R}^{l_{h,K}}.$$

Also, let $\mathbf{F}_{h,K} \in \mathbb{R}^{m_{h,K}+l_{h,K}}$ be the local right hand side vector given by the stabilized linear form $F_K(\cdot)$ defined in (42) and $\mathbf{B}_{h,K} \in \mathbb{R}^{(m_{h,K}+l_{h,K})\times(m_{h,K}+l_{h,K})}$ the local rigidity matrix given by the stabilized bilinear form $B_K(\cdot\,;\cdot)$ defined in (41). They are both computed using the subspace $\mathbf{V}_h(K) \times Q_h(K)$. We denote by $\mathbf{I}^u \in \mathbb{R}^{m_{h,K}\times m_{h,K}}$ and $\mathbf{I}^p \in \mathbb{R}^{l_{h,K}\times l_{h,K}}$ the identity matrices, $\mathbf{0}^u \in \mathbb{R}^{l_{h,K}\times m_{h,K}}$ and $\mathbf{0}^p \in \mathbb{R}^{m_{h,K}\times l_{h,K}}$ the rectangular matrices composed of zeros, and

$$\boldsymbol{P}_K^u := \begin{bmatrix} \mathbf{I}^u \\ \mathbf{0}^u \end{bmatrix} \in \mathbb{R}^{(m_{h,K}+l_{h,K})\times m_{h,K}} \quad \text{and} \quad \boldsymbol{P}_K^p := \begin{bmatrix} \mathbf{0}^p \\ \mathbf{I}^p \end{bmatrix} \in \mathbb{R}^{(m_{h,K}+l_{h,K})\times l_{h,K}}.$$

Algorithm 1 MHM algorithm for Stokes

1: **for** For each $K \in \mathcal{T}_H$ **do**

2: For each $\boldsymbol{\psi}_j$ defined on ∂K solve

$$\mathbf{B}_{h,K} X_{j,K} = \boldsymbol{P}_K^u \boldsymbol{S}_{j,K}$$

3: For each $\boldsymbol{\psi}_i$, $\boldsymbol{\psi}_j$ defined on ∂K, $\boldsymbol{\phi}_i$ defined on K, and using the explicit solution of the local problems given by (52), compute the local matrices

$$\mathcal{A}_{h,K} := (a_{ij}^K), \qquad a_{ij}^K := \boldsymbol{S}_{i,K}^T (\boldsymbol{P}_K^u)^T \underbrace{\mathbf{B}_{h,K}^{-1} \boldsymbol{P}_K^u \boldsymbol{S}_{j,K}}_{X_{j,K}}$$

and

$$\mathcal{B}_{h,K} := (b_{1j}^K), \qquad b_{1j}^K := -\langle \boldsymbol{\psi}_j, \boldsymbol{\chi}_h^{\boldsymbol{u}} \rangle_{\partial K}$$

and

$$\mathcal{C}_{h,K} := (c_{ij}^K), \qquad c_{ij}^K := -\langle \boldsymbol{\psi}_j, \boldsymbol{\phi}_i \rangle_{\partial K}$$

4: Assemble $\mathcal{A}_{h,K}$, $\mathcal{B}_{h,K}$ and $\mathcal{C}_{h,K}$ into $\mathcal{A}$, $\mathcal{B}$ and $\mathcal{C}$, respectively

5: Solve

$$\mathbf{B}_{h,K} Y_K = \mathbf{F}_{h,K}$$

6: For each $\boldsymbol{\psi}_i$ defined on ∂K, and $\boldsymbol{\phi}_i$ defined on K, compute

$$\mathbf{F}_1^K = (f_i^{1,K}), \qquad f_i^{1,K} := \boldsymbol{S}_{i,K}^T (\boldsymbol{P}_K^u)^T \underbrace{\mathbf{B}_{h,K}^{-1} \mathbf{F}_{h,K}}_{Y_K} - (\boldsymbol{\psi}_i, \boldsymbol{g})_{\partial K \cap \partial \Omega}$$

and

$$F_2^K = (f^{2,K}), \qquad f^{2,K} := \boldsymbol{R}_K^T (\boldsymbol{P}_K^p)^T \underbrace{\mathbf{B}_{h,K}^{-1} \mathbf{F}_{h,K}}_{Y_K}$$

and

$$\mathbf{F}_3^K = (f_i^{3,K}), \qquad f_i^{3,K} := -(\boldsymbol{f}, \boldsymbol{\phi}_i)_K$$

7: Assemble $\mathbf{F}_1^K$, F_2^K and $\mathbf{F}_3^K$ into $\mathbf{F}_1$, F_2 and $\mathbf{F}_3$

8: **end for**

9: Define $\tilde{\mathcal{A}} := \mathcal{A} + \mathcal{B}^T \mathcal{D}^{-1} \mathcal{B}$ and $\tilde{\mathbf{F}}_1 := \mathbf{F}_1 + \mathcal{B}^T \mathcal{D}^{-1} F_2$, where $\mathcal{D}^{-1} = \dfrac{d}{\nu} |\Omega|^{-1}$, and solve the global problem

$$\begin{bmatrix} \tilde{\mathcal{A}} & \mathcal{C}^T \\ \mathcal{C} & \mathbf{0} \end{bmatrix} \begin{bmatrix} \vec{\boldsymbol{\lambda}} \\ \vec{\boldsymbol{u}}_0 \end{bmatrix} = \begin{bmatrix} \tilde{\mathbf{F}}_1 \\ \mathbf{F}_3 \end{bmatrix} \tag{54}$$

10: Compute, using (46), the solution of the two–level MHM method

$$\begin{aligned} \boldsymbol{u}_{H,h} &= \sum_{i=1}^{m_0} u_0^i \, \boldsymbol{\phi}_i + \sum_{i=1}^{m_\lambda} \lambda_i \left\{ \sum_{K \in \mathcal{T}_H} \sum_{j=1}^{m_{h,K}} X_{i,K}^j \, \boldsymbol{\xi}_j^K \right\} + \sum_{K \in \mathcal{T}_H} \sum_{j=1}^{m_{h,K}} Y_{i,K}^j \, \boldsymbol{\xi}_j^K \\ p_{H,h} &= \sum_{i=1}^{m_\lambda} \lambda_i \left\{ \sum_{K \in \mathcal{T}_H} \sum_{j=m_{h,K}+1}^{m_{h,K}+l_{h,K}} X_{i,K}^j \, q_j^K \right\} + \sum_{K \in \mathcal{T}_H} \sum_{j=m_{h,K}+1}^{m_{h,K}+l_{h,K}} Y_{i,K}^j \, q_j^K \\ \boldsymbol{\sigma}_{H,h} &= -\nu \, \nabla \boldsymbol{u}_{H,h} + p_{H,h} \mathbf{I} \end{aligned} \tag{55}$$

Remark 7. *Note that in the Brinkman case* $\mathbf{V}_0 = \{\mathbf{0}\}$*, the global discrete system* (51) *is reduced to solve*

$$\begin{bmatrix} \mathcal{A} & \mathcal{B}^T \\ \mathcal{B} & -\mathcal{D} \end{bmatrix} \begin{bmatrix} \vec{\boldsymbol{\lambda}} \\ \rho_0 \end{bmatrix} = \begin{bmatrix} \mathbf{F}_1 \\ F_2 \end{bmatrix}.$$

The underlying algorithm follows replacing (54) *by the above system and setting* $u_0^i = 0$ *in* (55)*.*

Next, we validate the MHM method (39) on a series of two-dimensional numerical tests. We start by assessing its convergence properties. Then, we validate the method with the lid-driven cavity problem, under a singular perturbed regime, and a highly heterogeneous media problem. We recall that the local problems are solved considering the USFEM in (40). If l is the order of the interpolation choice on faces, then we choose equal-order polynomial interpolation for the velocity and the pressure of order $l+2$, according to Lemma 3, if one single element is used in the second-level mesh.

3.1. Convergence assessment

We now consider the convergence properties of the MHM method (39) using one element sub-meshes. We first address the Stokes model, using a polynomial exact solution. Next, we perform the same study for the Brinkman model using an analytical solution with boundary layers.

3.1.1. The Stokes case

We consider problem (1) with $\nu = 1$ and $\boldsymbol{\gamma} = 0$ on the unit square domain, and the function $\boldsymbol{f}$ and the Dirichlet boundary conditions chosen such that the exact solution reads

$$u_1(x,y) = -256\, x^2(x-1)^2 y(y-1)(2y-1), \quad u_2(x,y) = -u_1(y,x), \quad p(x,y) = 150\,(x-\frac{1}{2})(y-\frac{1}{2}).$$

Figures 3–5 show the error of the velocity, the pressure, and the stress on their natural norms for different values of l. The degree l drives convergence. Observe the optimal convergence of $\|p - p_{H,h}\|_{0,\Omega}$ of order $\mathcal{O}(H^{l+1})$, and the super-convergence of $\|\boldsymbol{u} - \boldsymbol{u}_{H,h}\|_{0,\Omega}$ and $|\boldsymbol{u} - \boldsymbol{u}_{H,h}|_{1,\mathcal{T}_H}$, which converge of order $\mathcal{O}(H^{l+2})$ and $\mathcal{O}(H^{l+1})$, respectively. Also, the post-processed stress variable $\boldsymbol{\sigma}_{H,h}$ presents optimal convergence of order $\mathcal{O}(H^l)$ for $\|\boldsymbol{\sigma} - \boldsymbol{\sigma}_{H,h}\|_{\mathrm{div},\mathcal{T}_H}$. Hereafter, we denote $\|\cdot\|_{0,\Omega}$, $|\cdot|_{1,\mathcal{T}_H}$ and $\|\cdot\|_{\mathrm{div},\mathcal{T}_H}$ the $L^2(\Omega)$ norm, the $H^1(\mathcal{T}_H)$ semi-norm and the $H(\mathrm{div},\mathcal{T}_H)$ norm, respectively. Unexpectedly, we still recover convergence of order $\mathcal{O}(H)$ in the $H(\mathrm{div},\mathcal{T}_H)$ norm in the simplest case $l = 0$ (see Figure 3). As predicted by the theory, the MHM method conserves the mass locally as shown in Table 1.

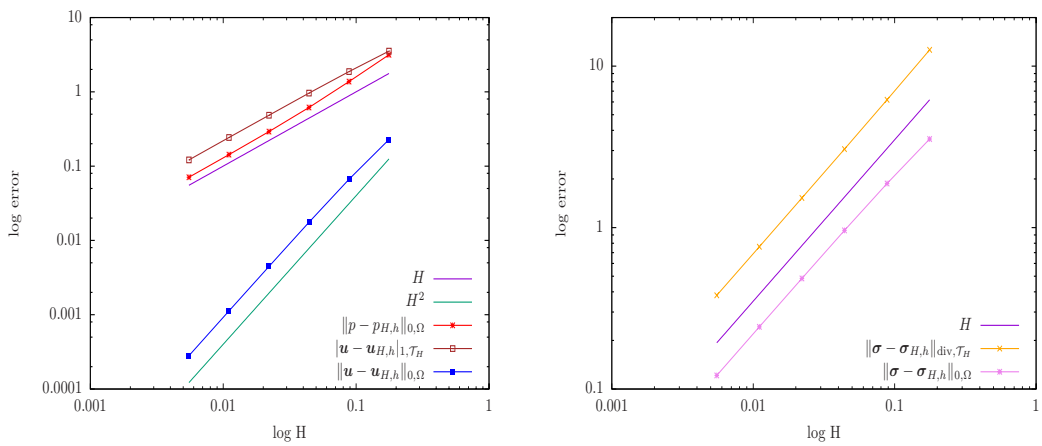

Figure 3: Convergence curves with $\boldsymbol{\Lambda}_0$.

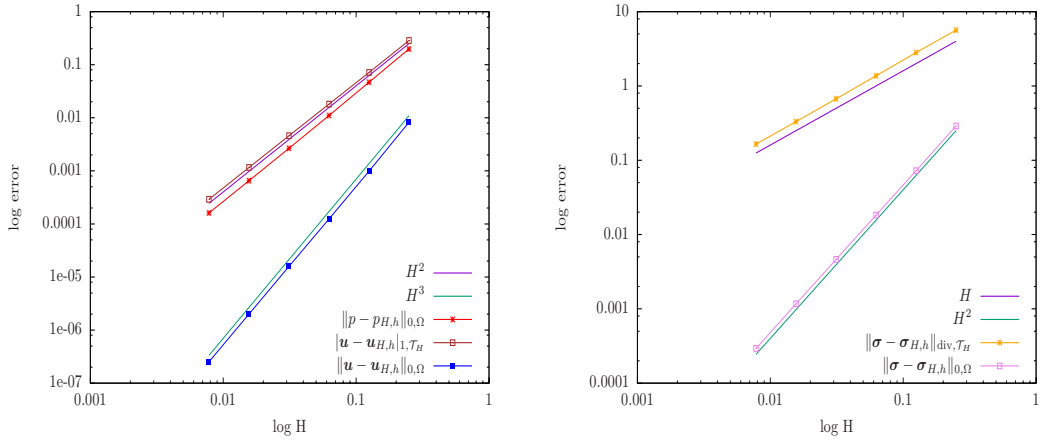

Figure 4: Convergence curves with $\mathbf{\Lambda}_1$.

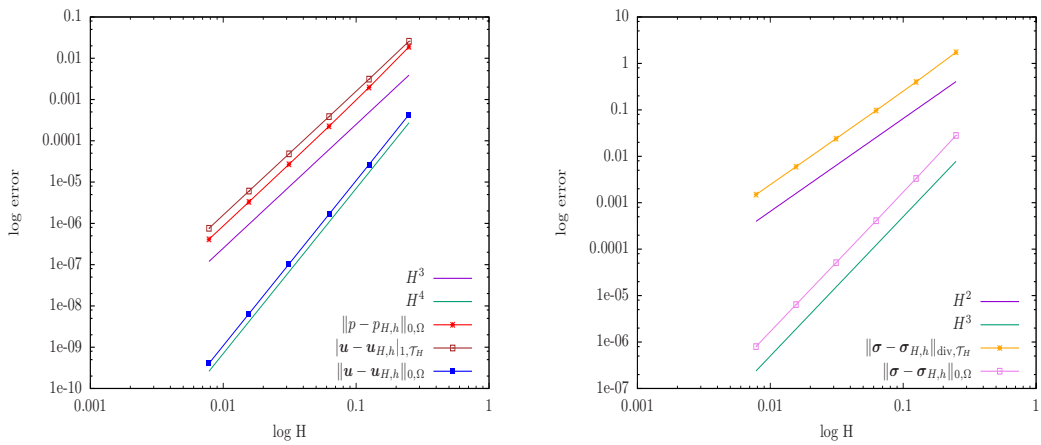

Figure 5: Convergence curves with $\mathbf{\Lambda}_2$.

H	$\mathbf{\Lambda}_0$	$\mathbf{\Lambda}_1$	$\mathbf{\Lambda}_2$
0.250	5.056e-17	1.4801e-16	1.1266e-16
0.125	2.4720e-17	7.0998e-17	7.1869e-17
6.25e-02	1.3487e-17	3.3093e-17	4.6540e-17
3.125e-02	7.2352e-18	1.8744e-17	2.3442e-17
1.5625e-02	3.5950e-18	9.2944e-18	1.4982e-17
7.8125e-03	2.1444e-18	5.4785e-18	7.9874e-18

Table 1: The loss of mass ($\max_{K\in\mathcal{T}_H} |\int_K \nabla\cdot\boldsymbol{u}_h\, d\boldsymbol{x}|$) is negligible for various mesh refinements.

3.1.2. The Brinkman case

This test case aims to measure the rate of convergence for a singularly perturbed problem. To this end, we let $\nu = 10^{-2}$ and $\boldsymbol{\gamma} = 1$. The domain is a unit square, and the function $\boldsymbol{f}$ and the Dirichlet boundary conditions are such that the exact solution is

$$u_1(x,y) = y - \frac{1-e^{y/\nu}}{1-e^{1/\nu}}, \quad u_2(x,y) = x - \frac{1-e^{x/\nu}}{1-e^{1/\nu}}, \quad p(x,y) = x - y.$$

We recover rates of convergence similar to the Stokes case (up to an expected loss of convergence on very coarse meshes due to the unresolved boundary layers). In fact, we found that $\|p - p_{H,h}\|_{0,\Omega}$ and $|\boldsymbol{u} - \boldsymbol{u}_{H,h}|_{1,\mathcal{T}_H}$ are of order $\mathcal{O}(H^{l+1})$ and $\|\boldsymbol{u} - \boldsymbol{u}_{H,h}\|_{0,\Omega}$ of order $\mathcal{O}(H^{l+2})$ (see Figures 6–8). Again, we notice the convergence of $\|\boldsymbol{\sigma} - \boldsymbol{\sigma}_{H,h}\|_{\mathrm{div},\mathcal{T}_H}$ for the stress variable $\boldsymbol{\sigma}_{H,h}$, and the surprising convergence of order $\mathcal{O}(H)$ when $l = 0$ (see Figure 6).

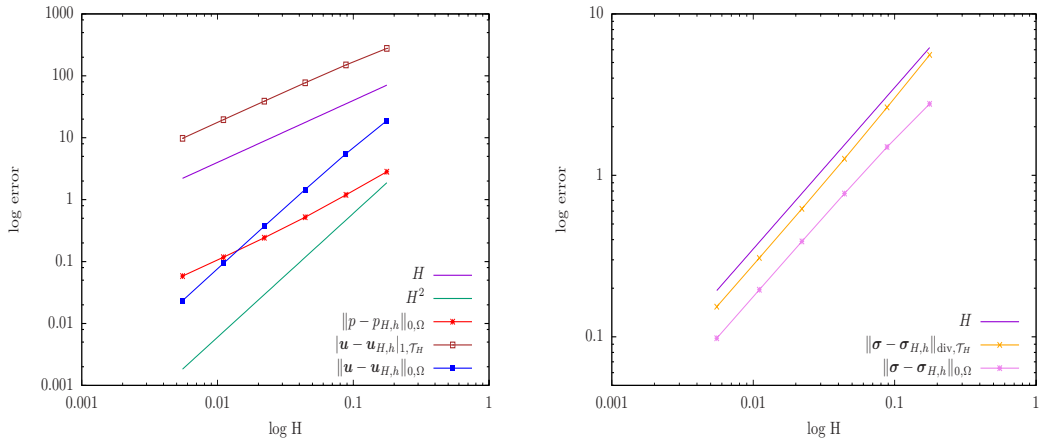

Figure 6: Convergence curves with $\boldsymbol{\Lambda}_0$.

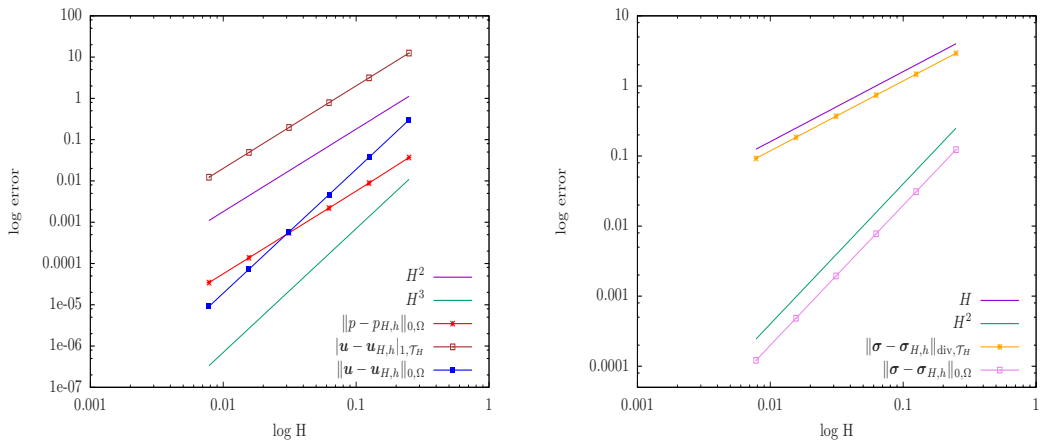

Figure 7: Convergence curves with $\boldsymbol{\Lambda}_1$.

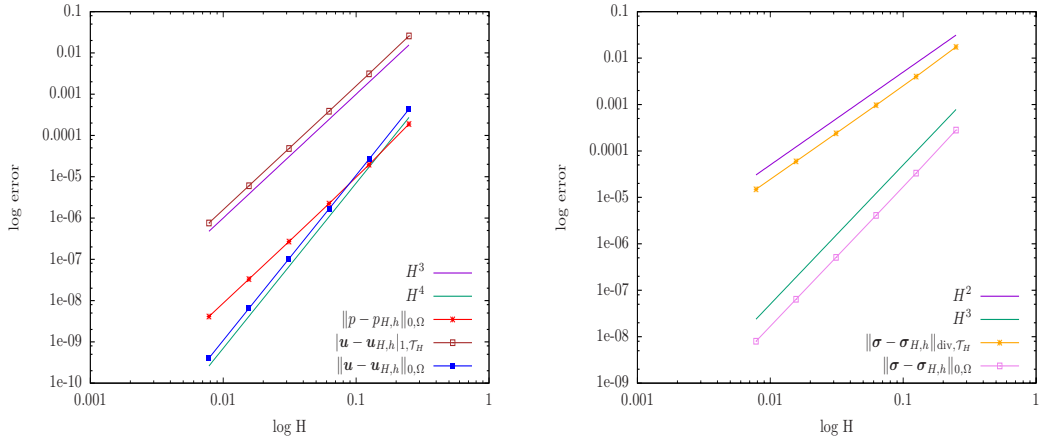

Figure 8: Convergence curves with $\mathbf{\Lambda}_2$.

In Table 2 we measure the local mass conservation property of the MHM method. The results are compared to the USFEM [10] using the pair $\mathbb{P}^2(K) \times \mathbb{P}^2(K)$. Notice that, as is usual for stabilized methods, mass is not conserved locally. Such a drawback is completely overcome by the MHM method on the coarse meshes, even though the USFEM itself is adopted at the second level.

H	$\mathbf{\Lambda}_0$	$\mathbf{\Lambda}_1$	$\mathbf{\Lambda}_2$	USFEM
0.250	7.7325e-16	9.3133e-16	1.1205e-15	1.8075e-02
0.125	5.8102e-16	1.3263e-15	1.4134e-15	5.5736e-03
6.25e-02	8.5168e-16	1.1898e-15	9.2654e-16	1.1326e-03
3.125e-02	1.0468e-15	1.2779e-15	1.3535e-15	1.4290e-04
1.5625e-02	1.2984e-15	1.3951e-15	1.2610e-15	1.3626e-05
7.8125e-03	1.2571e-15	1.2575e-15	1.3137e-15	1.1620e-06

Table 2: The loss of mass ($\max_{K\in\mathcal{T}_H} |\int_K \nabla\cdot\boldsymbol{u}_h\, d\boldsymbol{x}|$) is negligible for different mesh refinements. This feature is not shared by the USFEM with the pair of spaces $\mathbb{P}^2(K) \times \mathbb{P}^2(K)$ [10].

It is interesting to compare the accuracy between the MHM and the USFEM methods using the same order of approximation. To this end, we adopt the space $\mathbf{\Lambda}_1$ for the MHM method and the element $\mathbb{P}^2(K) \times \mathbb{P}^2(K)$ for the USFEM. We depict in Figure 9 the results, which shows that the solution from the MHM method is more accurate than the one from USFEM, no matter which norm is used to measure the error.

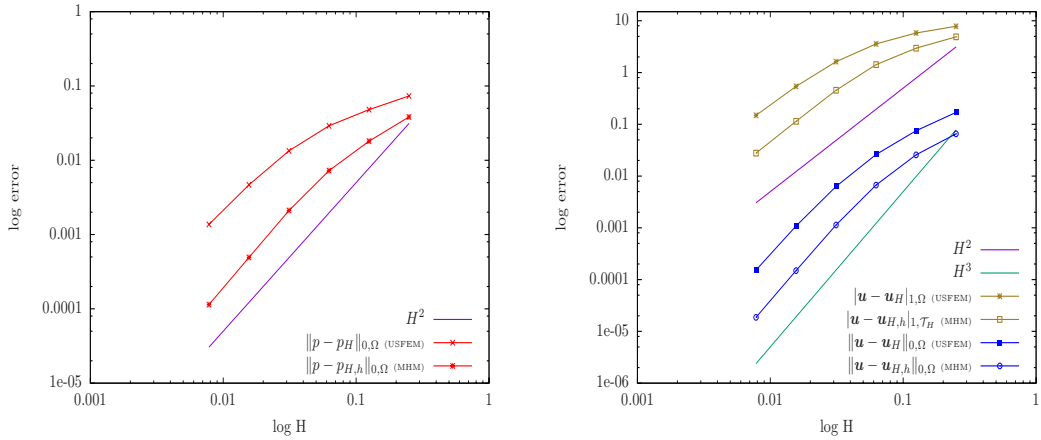

Figure 9: Comparison between the MHM (with the space $\boldsymbol{\Lambda}_1$) and the USFEM methods (with the pair of spaces $\mathbb{P}^2(K)\times\mathbb{P}^2(K)$). We observe that the former is more precise in all norms.

3.2. The lid–driven cavity problem

This section addresses the standard lid-driven cavity problem solving the Stokes (i.e. $\boldsymbol{\gamma} = \mathbf{0}$) and the reactive dominated Brinkman model ($\boldsymbol{\gamma} = 10^4$ and $\nu = 1$). Here a coarse mesh of $4,096$ triangular elements is used with a one element sub-mesh at the second level. Figure 10 depicts the isolines of the velocity showing the expected behavior for both cases. Particularly, for the Brinkman case, we recover the expected sharp boundary layer at $y = 1$. We observe that the velocity profile at $x = 0.5$ is free of spurious oscillations despite the coarse mesh (see Figure 11). Also, we compare the solutions using different spaces for the MHM method, namely, $\boldsymbol{\Lambda}_1$, $\boldsymbol{\Lambda}_1^4$ and $\boldsymbol{\Lambda}_0^4$ using a sub-mesh with 144 elements of $\mathbb{P}^3(K) \times \mathbb{P}^3(K)$ type in the cases of $\boldsymbol{\Lambda}_1$ and $\boldsymbol{\Lambda}_1^4$, and $\mathbb{P}^2(K) \times \mathbb{P}^2(K)$ in the case of $\boldsymbol{\Lambda}_0^4$. We conclude from this comparison that it is more precise to set piecewise interpolations on faces rather than the entire face, and also, low-order interpolation may be enough to approximate them. This is in agreement with the findings in [26] for reactive-advective dominated problems. Adopting the space $\boldsymbol{\Lambda}_1$ and a sub-mesh at the second level with 64 elements of $\mathbb{P}^1(K) \times \mathbb{P}^1(K)$ type, we observe equivalent results when compared to the one obtained using $\boldsymbol{\Lambda}_1$ on single-element sub-meshes (with $\mathbb{P}^3(K) \times \mathbb{P}^3(K)$). This points out that equal-order interpolation for all variables can be used within the MHM method as mentioned in Remark 4.

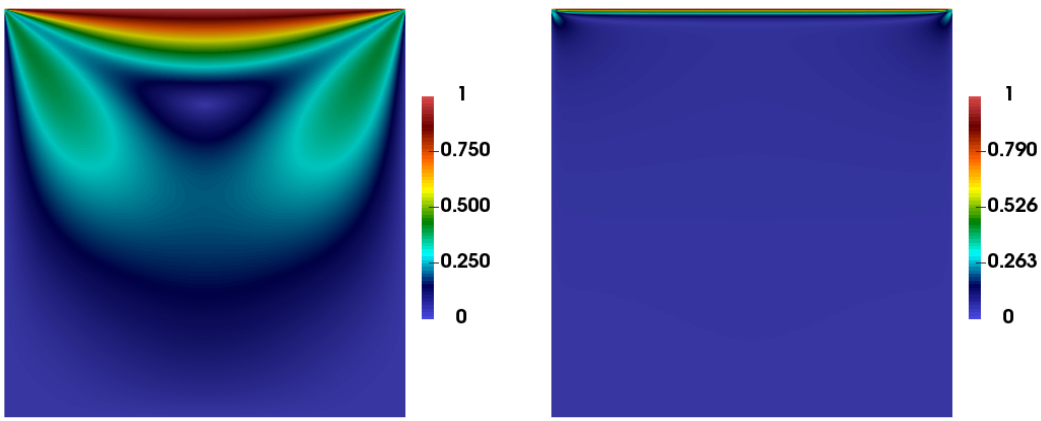

Figure 10: Isolines of $|\boldsymbol{u}_{H,h}|$ with $\boldsymbol{\Lambda}_0$ on a mesh with 4,096 elements. On the left is the solution with $\boldsymbol{\gamma} = 0$ (Stokes) and on the right with $\boldsymbol{\gamma} = 10^4$ (Brinkman). In both cases $\nu = 1$.

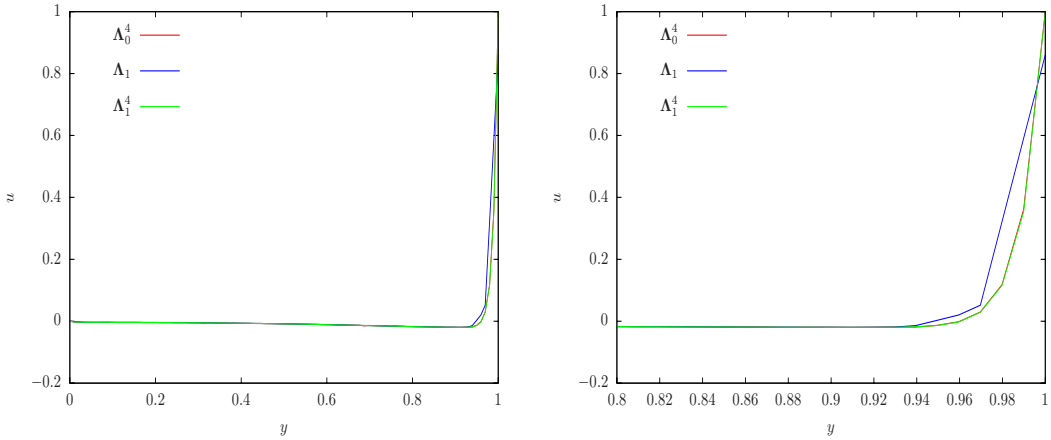

Figure 11: Profile of the tangential velocity at $x = 0.5$ (left) and a zoom of the profile (right). Note that using $\mathbf{\Lambda}_0^4$ on each face yields a better approximation compared to use $\mathbf{\Lambda}_1$ on the face. Here $\nu = 1$ and $\boldsymbol{\gamma} = 10^4$.

3.3. A highly heterogeneous case

This final numerical test illustrates the capacity of the MHM method to simulate a fluid flow with a highly heterogenous porous media on top of a coarse mesh. Indeed, such a domain (see Figure 12 for the permeability field) represents a quite realistic prototype of a reservoir. In this context, we adopt the following version of the Brinkman model

$$-\mu\,\Delta\boldsymbol{u} + \mu^*\mathcal{K}^{-1}\,\boldsymbol{u} + \nabla p \;=\; \mathbf{0} \quad \text{in } \Omega, \qquad \nabla\cdot\boldsymbol{u} \;=\; 0 \quad \text{in } \Omega, \tag{56}$$

where $\mathcal{K}$ is the permeability tensor, μ is the fluid viscosity, and μ^* is the so-called *effective* viscosity of the fluid. Generally, the value of μ^* depends on the properties of the porous medium. For example, if there are large variations in the material properties, μ^* might not be considered a homogeneous coefficient. Nevertheless, it is often assumed that such an effective viscosity is homogeneous, and that $\mu = \mu^*$.

Here, we assume that $\Omega :=]0,5[\times]0,1[$, $\mu = \mu^* = 10^{-4}$, the permeability tensor $\mathcal{K}$ is given in Figure 12, and we prescribe Dirichlet boundary conditions. Since the exact solution is not available, we propose a reference solution by solving the problem using the USFEM on a one million element mesh with the $\mathbb{P}^1(K)/\mathbb{P}^1(K)$ element.

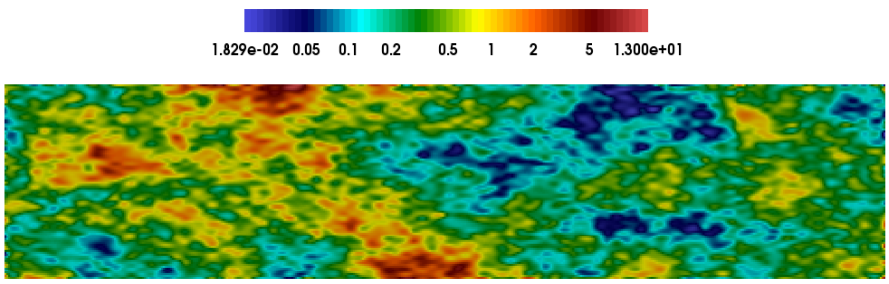

Figure 12: The permeability field $\mathcal{K}$ plotted on a logarithmic scale. The domain has physical dimensions equal to 5×1 cm. The permeability is given on a regular grid of 500×100 cells.

We carry out the computations using the MHM method with the space $\mathbf{\Lambda}_1^6$ on a structured coarse mesh of $1,290$ elements. The sub-meshes are composed of 36 elements of $\mathbb{P}^3(K) \times \mathbb{P}^3(K)$ type. The mesh is depicted in Figure 13. We notice in Figure 14, which is a magnified portion of the permeability field, that

the coarse mesh is not aligned with the changing in coefficients, and then, multiple scales remain within the elements and there are jumps in the coefficient across faces.

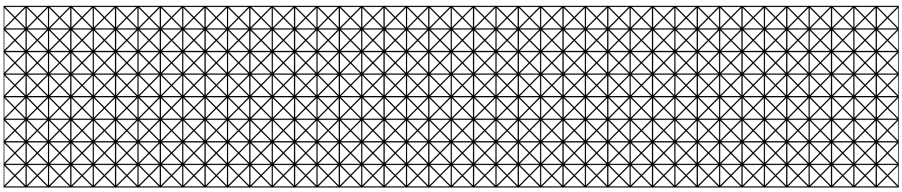

Figure 13: The mesh with $1,280$ elements.

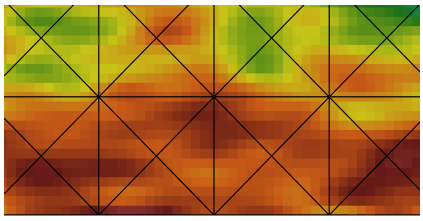

Figure 14: Magnification of the permeability field overlaid with the coarse mesh.

In Figures 15 and 17, we compare the absolute value of the velocity and pressure from the MHM method with their reference counterpart. We observe perfect agreement between the solutions. Also interesting, we observe that the MHM method captures perfectly changes across coarse mesh faces, as shown in the magnified plot of the absolute value of the velocity in Figure 16.

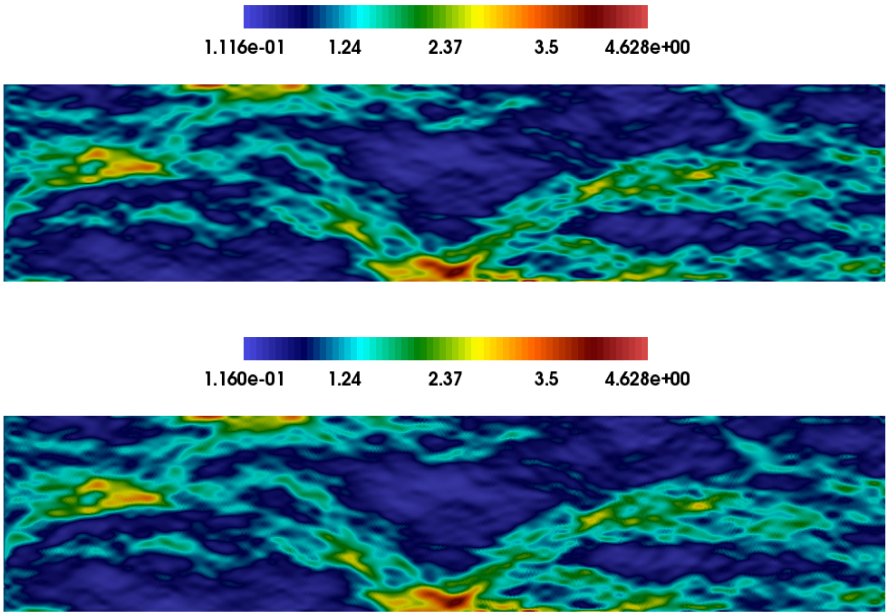

Figure 15: Isovalues of the absolute value of the velocity from the USFEM (top) and the MHM method (bottom).

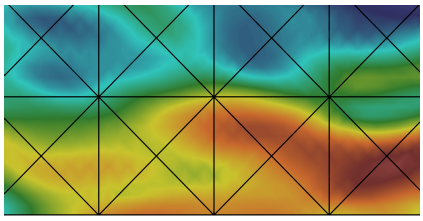

Figure 16: Magnified plot of the absolute value of the velocity from the MHM method with the corresponding mesh.

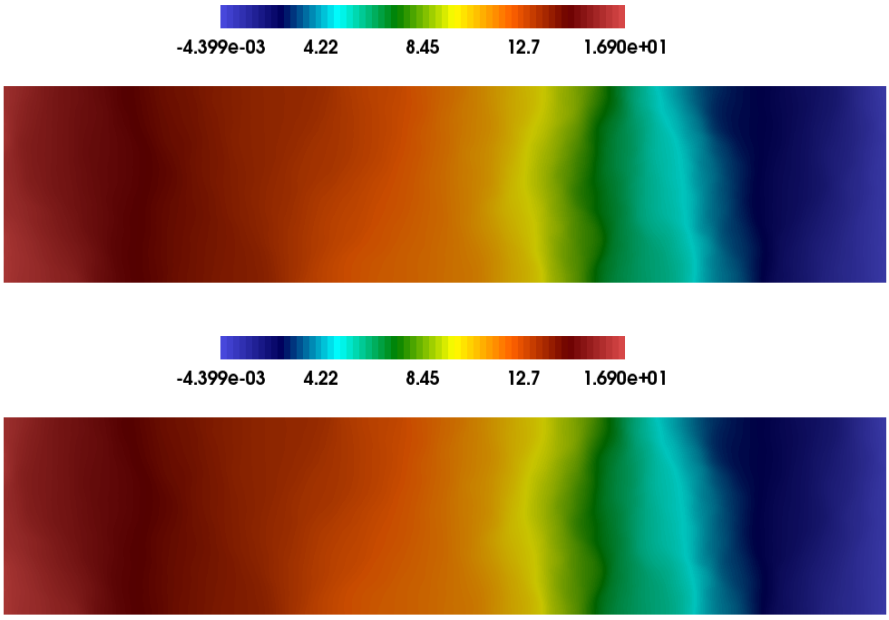

Figure 17: Isovalues of the pressure from the USFEM (top) and the MHM method (bottom).

4. Conclusion

The MHM method, first presented in [25], has been extended to the Stokes and Brinkman equations with highly heterogenous coefficients with the desirable property of local conservation. The method is based on the solution of independent local problems, which can be naturally solved using parallel facilities, and a global problem posed on the skeleton of a coarse mesh. Numerical tests verify that the new method yields optimal convergence for the primal (velocity and pressure) and the dual (stress) variables, with the upshot of achieving super-convergence for the velocity. Also, the MHM method shows great accuracy when approximating sharp boundary layers and highly heterogeneous coefficients on non-aligned meshes. We conclude that the MHM method, is well suited to parallel computing and to handling realistic multiscale boundary value problems with precision on coarse meshes. The numerical analysis of the proposed method is currently in progress [5] and preliminary theoretical results validate the numerics presented in this work. In addition, the cost-effectiveness of the present method, compared to other domain decomposition methodologies, deserves a detailed investigation.

Acknowledgements

The first author was partially founded by CONICYT/Chile through FONDECYT project N° 1150174, Basal project CMM–CI2MA PFB–03, Anillo project ACT1118 (ANANUM); and Red Doctoral REDOC.CTA, MINEDUC project UCO1202 at Universidad de Concepción. The third author was partially supported by CONICYT/Chile through FONDECYT project N° 11130674. The forth author was founded by CNPq/Brazil. These research results have received funding from the EU H2020 Programme and from MCTI/RNP-Brazil under the HPC4E Project, grant agreement N° 689772.

Appendix A.

In this appendix, we present some auxiliary results and address the proof of Theorems 1 and 2.

Lemma 4. *A continuous linear functional L on space $\mathbf{V}$ vanishes on $H_0^1(\Omega)^d$ if and only if there exist a unique element $\boldsymbol{\mu} \in \boldsymbol{\Lambda}$ such that*

$$L(\boldsymbol{v}) = (\boldsymbol{\mu}, \boldsymbol{v})_{\partial \mathcal{T}_H} \quad \textit{for all } \boldsymbol{v} \in \mathbf{V}.$$

Moreover, it holds

$$H_0^1(\Omega)^d = \{\boldsymbol{v} \in \mathbf{V} \,:\, (\boldsymbol{\mu}, \boldsymbol{v})_{\partial \mathcal{T}_H} = 0 \quad \textit{for all } \boldsymbol{\mu} \in \boldsymbol{\Lambda}\}.$$

Proof. Following closely Lemma 1 and Equation (2.12) in [34] the result follows.

Lemma 5. *A continuous linear functional L on space Q vanishes on $L_0^2(\Omega)$ if and only if there exist a unique element $\rho \in \mathbb{R}$ such that*

$$L(q) = (\rho, q)_Q \quad \textit{for all } q \in Q.$$

Proof. Suppose L is a bounded linear functional on Q that vanishes on $L_0^2(\Omega)$. By the Riesz Representation Theorem, there exists unique $\rho \in Q$ such that $L(q) = (\rho, q)_Q$ for all $q \in Q$. Therefore,

$$(\rho, q)_Q = L(q) = 0 \quad \text{for all } q \in L_0^2(\Omega).$$

It immediately follows that $\rho \in (L_0^2(\Omega))^\perp = \mathbb{R}$. On the other hand, given $\rho \in \mathbb{R} \subset Q$, it follows that $(\rho, q)_Q$ is a continuous linear functional vanishing on $L_0^2(\Omega)$.

Owing to the previous results, we now proof Theorem 1 and Theorem 2.

Theorem 6. *The function $(\boldsymbol{u}, p) \in H^1(\Omega)^d \times L_0^2(\Omega)$ is the unique solution of (3) if and only if $(\boldsymbol{u}, p, \boldsymbol{\lambda}, \rho) \in \mathbf{V} \times Q \times \boldsymbol{\Lambda} \times \mathbb{R}$ is the unique solution of (13) Moreover, $\rho = 0$ and it holds*

$$\boldsymbol{\lambda} = \boldsymbol{\sigma}\, \boldsymbol{n}^K\,|_{\partial K} \quad \textit{for all } K \in \mathcal{T}_h.$$

Proof. Let $(\boldsymbol{u}, p)$ be the solution of (3), and define the linear functional $L : \mathbf{V} \to \mathbb{R}$ by

$$L(\boldsymbol{v}) := (\boldsymbol{f}, \boldsymbol{v})_{\mathcal{T}_H} - (\nu\, \nabla \boldsymbol{u}, \nabla \boldsymbol{v})_{\mathcal{T}_H} - (\boldsymbol{\gamma}\, \boldsymbol{u}, \boldsymbol{v})_{\mathcal{T}_H} + (p, \nabla \cdot \boldsymbol{v})_{\mathcal{T}_H} \quad \text{for all } \boldsymbol{v} \in \mathbf{V}.$$

It follows that L is continuous on $\mathbf{V}$ and that L vanishes on $H_0^1(\Omega)^d$. Owing to Lemma 4, there exists a unique $\boldsymbol{\lambda} \in \boldsymbol{\Lambda}$ such that $L(\boldsymbol{v}) = (\boldsymbol{\lambda}, \boldsymbol{v})_{\partial \mathcal{T}_H}$ for all $\boldsymbol{v} \in \mathbf{V}$, and the first equation in (13) holds. Moreover, integrating by parts we get

$$\sum_{K \in \mathcal{T}_H} (\boldsymbol{\lambda}, \boldsymbol{v})_{\partial K} = \sum_{K \in \mathcal{T}_H} \big\{ (\boldsymbol{f} - (\nabla \cdot \boldsymbol{\sigma} + \boldsymbol{\gamma}\, \boldsymbol{u}), \boldsymbol{v})_K + (\boldsymbol{\sigma}\, \boldsymbol{n}^K, \boldsymbol{v})_{\partial K} \big\} = \sum_{K \in \mathcal{T}_H} (\boldsymbol{\sigma}\, \boldsymbol{n}^K, \boldsymbol{v})_{\partial K},$$

where we used that $(\boldsymbol{f} - (\nabla \cdot \boldsymbol{\sigma} + \boldsymbol{\gamma}\, \boldsymbol{u}), \boldsymbol{v})_{\mathcal{T}_H} = 0$. Then, it holds that $\boldsymbol{\sigma}\, \boldsymbol{n}^K\,|_{\partial K} = \boldsymbol{\lambda}$ for all $K \in \mathcal{T}_H$. Similarly, since $(\nabla \cdot \boldsymbol{u}, q)_{\mathcal{T}_H} = (\nabla \cdot \boldsymbol{u}, q)_\Omega = 0$ for all $q \in L_0^2(\Omega)$, Lemma 5 guarantees existence of a unique $\rho \in \mathbb{R}$ such

that $(\nabla\cdot\boldsymbol{u},q)_{\mathcal{T}_H}=(\rho,q)_\Omega$ for all $q\in Q$, and then the second equation in (13) holds. Also, using $\boldsymbol{u}\in H^1(\Omega)^d$ and $\boldsymbol{u}=\boldsymbol{g}$ on $\partial\Omega$, and integrating by parts, we get

$$\|\rho\|_{0,\Omega}^2=\sum_{K\in\mathcal{T}_H}(\boldsymbol{u}\cdot\boldsymbol{n}^K,\rho)_{\partial K}=(\boldsymbol{u}\cdot\boldsymbol{n},\rho)_{\partial\Omega}=(\boldsymbol{g}\cdot\boldsymbol{n},\rho)_{\partial\Omega}\,.$$

By the compatibility condition $(\boldsymbol{g}\cdot\boldsymbol{n},\rho)_{\partial\Omega}=0$, it then follows that $\rho=0$. Next, take $\boldsymbol{q}\in H(\mathrm{div},\Omega)$ and define $\boldsymbol{\mu}=\boldsymbol{q}\,\boldsymbol{n}^K$ on ∂K for all $K\in\mathcal{T}_H$. As such, using $\boldsymbol{u}=\boldsymbol{g}$ on $\partial\Omega$ we get

$$(\boldsymbol{\mu},\boldsymbol{u})_{\partial\mathcal{T}_H}=(\boldsymbol{q},\nabla\boldsymbol{u})_{\mathcal{T}_H}+(\nabla\cdot\boldsymbol{q},\boldsymbol{u})_{\mathcal{T}_H}=(\boldsymbol{q},\nabla\boldsymbol{u})_\Omega+(\nabla\cdot\boldsymbol{q},\boldsymbol{u})_\Omega=(\boldsymbol{q}\,\boldsymbol{n},\boldsymbol{u})_{\partial\Omega}=(\boldsymbol{\mu},\boldsymbol{g})_{\partial\Omega},$$

and we have the third equation in (13). The fourth equation in (13) follows from the fact the $p\in L_0^2(\Omega)$. We conclude that $(\boldsymbol{u},p,\boldsymbol{\lambda},\rho)\in\mathbf{V}\times Q\times\boldsymbol{\Lambda}\times\mathbb{R}$ is the unique solution of (13) with $\rho=0$ and $\boldsymbol{\lambda}=\sigma\,\boldsymbol{n}^K|_{\partial K}$.

Conversely, let $(\boldsymbol{u},p,\boldsymbol{\lambda},0)\in\mathbf{V}\times Q\times\boldsymbol{\Lambda}\times\mathbb{R}$ be the unique solution of (13). Then it is clear, using the last equation of (13), that $p\in L_0^2(\Omega)$. Let $\boldsymbol{u_g}\in H^1(\Omega)^d$, such that $\boldsymbol{u_g}=\boldsymbol{g}$ on $\partial\Omega$. Then $\boldsymbol{u}-\boldsymbol{u_g}\in\mathbf{V}$ and, from the third equation of (13), $(\boldsymbol{\mu},\boldsymbol{u}-\boldsymbol{u_g})_{\partial\mathcal{T}_H}=0$ for all $\boldsymbol{\mu}\in\boldsymbol{\Lambda}$. Thus, from Lemma 4, we have that $\boldsymbol{u}-\boldsymbol{u_g}\in H_0^1(\Omega)^d$ and then $\boldsymbol{u}\in H^1(\Omega)^d$ with $\boldsymbol{u}=\boldsymbol{g}$ on $\partial\Omega$. Now, using the second equation of (13), with $q\in L_0^2(\Omega)$, we get that $(\nabla\cdot\boldsymbol{u},q)_\Omega=0$. Also, the first equation of (13) implies, using Lemma 4, we get

$$(\nu\,\nabla\boldsymbol{u},\nabla\boldsymbol{v})_\Omega+(\boldsymbol{\gamma}\,\boldsymbol{u},\boldsymbol{v})_\Omega-(p,\nabla\cdot\boldsymbol{v})_\Omega=(\boldsymbol{f},\,\boldsymbol{v})_\Omega,$$

for all $\boldsymbol{v}\in H_0^1(\Omega)^d$. Therefore, $(\boldsymbol{u},p)\in H^1(\Omega)^d\times L_0^2(\Omega)$ is the unique solution to (3).

Theorem 7. *Consider $\boldsymbol{f}\in L^2(\Omega)^d$ and $\boldsymbol{g}\in H^{1/2}(\partial\Omega)^d$ with $\int_{\partial\Omega}\boldsymbol{g}\cdot\boldsymbol{n}\,d\boldsymbol{s}=0$. Problem (13) admits a unique solution $(\boldsymbol{u},p,\boldsymbol{\lambda},0)\in\mathbf{V}\times Q\times\boldsymbol{\Lambda}\times\mathbb{R}$ if and only if problem (21) admits a unique solution $(\boldsymbol{u}_0,\boldsymbol{\lambda},0)\in\mathbf{V}_0\times\boldsymbol{\Lambda}\times\mathbb{R}$. Moreover, the following characterizations holds:*

$$\boldsymbol{u}\;=\;\boldsymbol{u}_0\;+\;\boldsymbol{u}^{\boldsymbol{\lambda}}+\boldsymbol{u}^{\boldsymbol{f}}\quad\textit{and}\quad p\;=\;p^{\boldsymbol{\lambda}}+p^{\boldsymbol{f}}.$$

Proof. Let $(\boldsymbol{u},p,\boldsymbol{\lambda},0)\in\mathbf{V}\times Q\times\boldsymbol{\Lambda}\times\mathbb{R}$ be the unique solution of problem (13). Then, there exists a unique $\boldsymbol{u}_0\in\mathbf{V}_0$ and $\boldsymbol{u}_0^\perp\in\mathbf{V}_0^\perp$ such that $\boldsymbol{u}=\boldsymbol{u}_0+\boldsymbol{u}_0^\perp$. Taking $\boldsymbol{v}=\boldsymbol{v}_0\in\mathbf{V}_0$ in the first equation of (13), we get

$$(\boldsymbol{\lambda},\boldsymbol{v}_0)_{\partial\mathcal{T}_H}=(\boldsymbol{f},\,\boldsymbol{v}_0)_{\mathcal{T}_H}\quad\text{for all }\boldsymbol{v}_0\in\mathbf{V}_0,$$

and the first equation in (21) is satisfied. Next, given $K\in\mathcal{T}_H$, we select $(\boldsymbol{v},\boldsymbol{\mu},\xi)=(\boldsymbol{v}_0^\perp|_K,0,0)$ in (13) to get

$$\begin{cases}a_K(\boldsymbol{u}_0^\perp,\boldsymbol{v})+b_K(\boldsymbol{v}_0^\perp,p)=-\langle\boldsymbol{\lambda},\boldsymbol{v}_0^\perp\rangle_{\partial K}+(\boldsymbol{f},\,\boldsymbol{v}_0^\perp)_K\quad\text{for all }\boldsymbol{v}_0^\perp\in\mathbf{V}_0^\perp(K),\\ \qquad\qquad b_K(\boldsymbol{u}_0^\perp,q)=0\quad\text{for all }q\in Q(K).\end{cases}$$

Thereby, from the uniqueness of the solution of local problems (22) and (23), we arrive at $\boldsymbol{u}_0^\perp=\boldsymbol{u}^{\boldsymbol{\lambda}}+\boldsymbol{u}^{\boldsymbol{f}}$ and $p=p^{\boldsymbol{\lambda}}+p^{\boldsymbol{f}}$. Using such a characterization in the third and fourth equations in (13), we obtain the second and third equations of (21). We conclude that $(\boldsymbol{u}_0,\boldsymbol{\lambda},0)$ is the unique solution of (21).

Conversely, assume that (21) admits a unique solution $(\boldsymbol{u}_0,\boldsymbol{\lambda},0)\in\mathbf{V}_0\times\boldsymbol{\Lambda}\times\mathbb{R}$. Pick $(\boldsymbol{u},p)\in\mathbf{V}\times Q$ the functions defined by

$$\boldsymbol{u}=\boldsymbol{u}_0+\boldsymbol{u}^{\boldsymbol{\lambda}}+\boldsymbol{u}^{\boldsymbol{f}}\quad\text{and}\quad p=p^{\boldsymbol{\lambda}}+p^{\boldsymbol{f}}.\tag{A.1}$$

From the second and third equations of (21), it is easily seen that $\boldsymbol{u}$ and p satisfy, respectively,

$$(\boldsymbol{\mu},\boldsymbol{u})_{\partial\mathcal{T}_H}=(\boldsymbol{\mu},\boldsymbol{g})_{\partial\Omega}\quad\text{for all }\boldsymbol{\mu}\in\boldsymbol{\Lambda},$$

and

$$(\xi,p)_\Omega=0\quad\text{for all }\xi\in\mathbb{R}.$$

Now, using equations (22) and (23), the definition of $\boldsymbol{u}$ and p in (A.1) and the first equation in (21), it holds

$$\begin{aligned} a(\boldsymbol{u},\boldsymbol{v}) + b(\boldsymbol{v},p) + (\boldsymbol{\lambda},\boldsymbol{v})_{\partial\mathcal{T}_H} &= a(\boldsymbol{u}^{\boldsymbol{\lambda}} + \boldsymbol{u}^{\boldsymbol{f}}, \boldsymbol{v}_0^{\perp}) + b(\boldsymbol{v}_0^{\perp}, p^{\boldsymbol{\lambda}} + p^{\boldsymbol{f}}) + (\boldsymbol{\lambda},\boldsymbol{v}_0)_{\partial\mathcal{T}_H} + (\boldsymbol{\lambda},\boldsymbol{v}_0^{\perp})_{\partial\mathcal{T}_H} \\ &= -(\boldsymbol{\lambda},\boldsymbol{v}_0^{\perp})_{\partial\mathcal{T}_H} + (\boldsymbol{f},\boldsymbol{v}_0^{\perp})_{\mathcal{T}_H} + (\boldsymbol{\lambda},\boldsymbol{v}_0)_{\partial\mathcal{T}_H} + (\boldsymbol{\lambda},\boldsymbol{v}_0^{\perp})_{\partial\mathcal{T}_H} \\ &= (\boldsymbol{f},\boldsymbol{v})_{\mathcal{T}_H}, \end{aligned}$$

for all $\boldsymbol{v} \in \mathbf{V}$, and the first equation in (13) is satisfied. Using again equations (22) and (23), the definition of $\boldsymbol{u}$ and p in (A.1) and the fact that, from Theorem 6 it holds $\rho = 0$, we get

$$b(\boldsymbol{u}, q) = b(\boldsymbol{u}^{\boldsymbol{\lambda}} + \boldsymbol{u}^{\boldsymbol{f}}, q) = 0,$$

for all $q \in Q$. We conclude that $(\boldsymbol{u}, p, \boldsymbol{\lambda}) \in \mathbf{V} \times Q \times \boldsymbol{\Lambda}$ given in (A.1) is the unique solution of (13).

References

[1] Abdulle, A., Budac, O., 2015. An adaptive finite element heterogeneous multiscale method for Stokes flow in porous media. SIAM Multiscale Model. and Simul. 13 (1), 256–290.

[2] Agouzal, A., Thomas, J. M., 1995. Une méthode d'eléments finis hybrides en décomposition de domaines. RAIRO-Math Model Num. 29 (6), 749–765.

[3] Araya, R., Barrenechea, G. R., Valentin, F., 2006. Stabilized finite element methods based on multiscale enrichment for the Stokes problem. SIAM J. Numer. Anal. 44 (1), 322–348.

[4] Araya, R., Harder, C., Paredes, D., Valentin, F., 2013. Multiscale hybrid-mixed method. SIAM J. Numer. Anal. 51 (6), 3505–3531.

[5] Araya, R., Harder, C., Poza, A., Valentin, F., 2016. Multiscale hybrid-mixed method for the Stokes and Brinkman equations – The analysis, in preparation.

[6] Arbogast, T., Boyd, K., 2006. Subgrid upscaling and mixed multiscale finite elements. SIAM J. Numer. Anal. 44 (3), 1150–1171.

[7] Arbogast, T., Pencheva, G., Wheeler, M. F., Yotov, I., 2007. A multiscale mortar mixed finite element method. SIAM Multiscale Model. and Simul. 6 (1), 319–346.

[8] Arnold, D. N., Brezzi, F., 1985. Mixed and nonconforming finite element methods: Implementation, postprocessing and error estimates. RAIRO-Math Model Num. 19 (1), 7–32.

[9] Babuska, I., Osborn, E., 1983. Generalized finite element methods: Their performance and their relation to mixed methods. SIAM J. Num. Anal. 20 (3), 510–536.

[10] Barrenechea, G. R., Valentin, F., 2002. An unusual stabilized finite element method for a generalized Stokes problem. Numer. Math. 92 (4), 653–677.

[11] Brezzi, F., Fortin, M., 1991. Mixed and hybrid finite element methods. Vol. 15 of Springer Series in Computational Mathematics. Springer-Verlag, Berlin, New-York.

[12] Brezzi, F., Fortin, M., 2001. A minimal stabilisation procedure for mixed finite element methods. Numer. Math. 89 (3), 457–492.

[13] Brezzi, F., Franca, L. P., Hughes, T. J. R., Russo, A., 1997. Stabilization techniques and subgrid scales capturing. In: The state of the art in numerical analysis. Vol. 63 of Inst. Math. Appl. Conf. Ser. New Ser. Oxford Univ. Press, New-York, pp. 391–406.

[14] Brezzi, F., Marini, D., 2000. Error estimates for the three-field formulation with bubble stabilization. Math. Comp. 70 (235), 911–934.

[15] Brezzi, F., Marini, L. D., 1994. A three-field domain decomposition method. In: et al., A. Q. (Ed.), Domain Decomposition in Science and Engineering. American Mathematical Society, Providence, pp. 27–34.

[16] Cockburn, B., Gopalakrishnan, J., 2009. The derivation of Hybridizable Discontinuous Galerkin methods for Stokes flow. SIAM J. Numer. Anal. 47 (2), 1092–1125.

[17] Cockburn, B., Saya, F.-J., 2014. Divergence-conforming HDG methods for Stokes flows. Math. Comp. 83 (298), 1571–1598.

[18] E, W., Engquist, B., 2005. The Heterogeneous Multi-Scale Method for Homogenization Problems. In: Multiscale Methods in Science and Engineering. Springer Berlin Heidelberg, Berlin/Heidelberg, pp. 89–110.

[19] Efendiev, Y., Galvis, J., Hou, T. Y., 2013. Generalized multiscale finite element methods (GMsFEM). J. Comput. Phys. 251, 116–135.

[20] Efendiev, Y., Lazarov, R., Moon, M., Shi, K., 2015. A spectral multiscale hybridizable discontinuous Galerkin method for second order elliptic problems. Comput. Methods Appl. Mech. Engrg. 292, 243–256.

[21] Farhat, C., Harari, I., Franca, L. P., 2001. The discontinuous enrichment method. Comput. Methods Appl. Mech. Engrg. 190 (48), 6455–6479.

[22] Girault, V., Vassilev, D., Yotov, I., 2014. Mortar multiscale finite element methods for Stokes–Darcy flows. Numer. Math. 165, 93–165.

[23] Gopalakrishnan, J., Qiu, W., 2014. An analysis of the practical DPG method. Math. Comp. 83 (286), 537–552.

[24] Harder, C., Madureira, A. L., Valentin, F., 2016. A hybrid-mixed method for elasticity. ESAIM: Math. Model. Num. Anal. 50 (2), 311–336.

[25] Harder, C., Paredes, D., Valentin, F., 2013. A family of multiscale hybrid-mixed finite element methods for the Darcy equation with rough coefficients. J. Comput. Phys. 245, 107–130.
[26] Harder, C., Paredes, D., Valentin, F., 2015. On a multiscale hybrid-mixed method for advective-reactive dominated problems with heterogenous coefficients. SIAM Multiscale Model. and Simul. 13 (2), 491–518.
[27] Harder, C., Valentin, F., 2016. Foundations of the MHM method. In: Barrenechea, G. R., Brezzi, F., Cangiani, A., Georgoulis, E. H. (Eds.), Building Bridges: Connections and Challenges in Modern Approaches to Numerical Partial Differential Equations. Lecture Notes in Computational Science and Engineering. Springer.
[28] Hou, T. Y., Wu, X., Cai, Z., 1999. Convergence of a multiscale finite element method for elliptic problems with rapidly oscillating coefficients. Math. Comp. 68 (227), 913–943.
[29] Hughes, T. J. R., 1995. Multiscale phenomena: Green's functions, the Dirichlet-to-Neumann formulation, subgrid scale models, bubbles and the origin of stabilized methods. Comput. Methods Appl. Mech. Engrg. 127 (1–4), 387–401.
[30] Hughes, T. J. R., Feijoo, G. R., Mazzei, L., Quincy, J., 1998. The variational multiscale method–A paradigm for computational mechanics. Comput. Methods Appl. Mech. Engrg. 166 (1–2), 3–24.
[31] Madureira, A., 2015. Abstract multiscale–hybrid–mixed methods. Calcolo 52 (4), 543–557.
[32] Malqvist, A., Peterseim, D., 2014. Localization of elliptic multiscale problems. Math. Comp. 83 (290), 2583–2603.
[33] Paredes, D., Valentin, F., Versieux, H. M., 2016. On the robusteness of multiscale hybrid-mixed methods, to appear in Math. Comp. DOI: 10.1090/mcom/3108.
[34] Raviart, P., Thomas, J., 1977. Primal hybrid finite element methods for 2nd order elliptic equations. Math. Comp. 31 (138), 391–413.
[35] Sangalli, G., 2003. Capturing small scales in elliptic problems using a Residual-Free Bubbles finite element method. SIAM Multiscale Model. Simul. 1 (3), 485–503.
[36] Wheeler, M. F., Xue, G., Yotov, I., 2012. A multiscale mortar multipoint flux mixed finite element method. Math. Models Methods Appl. Sci. 46, 759–796.